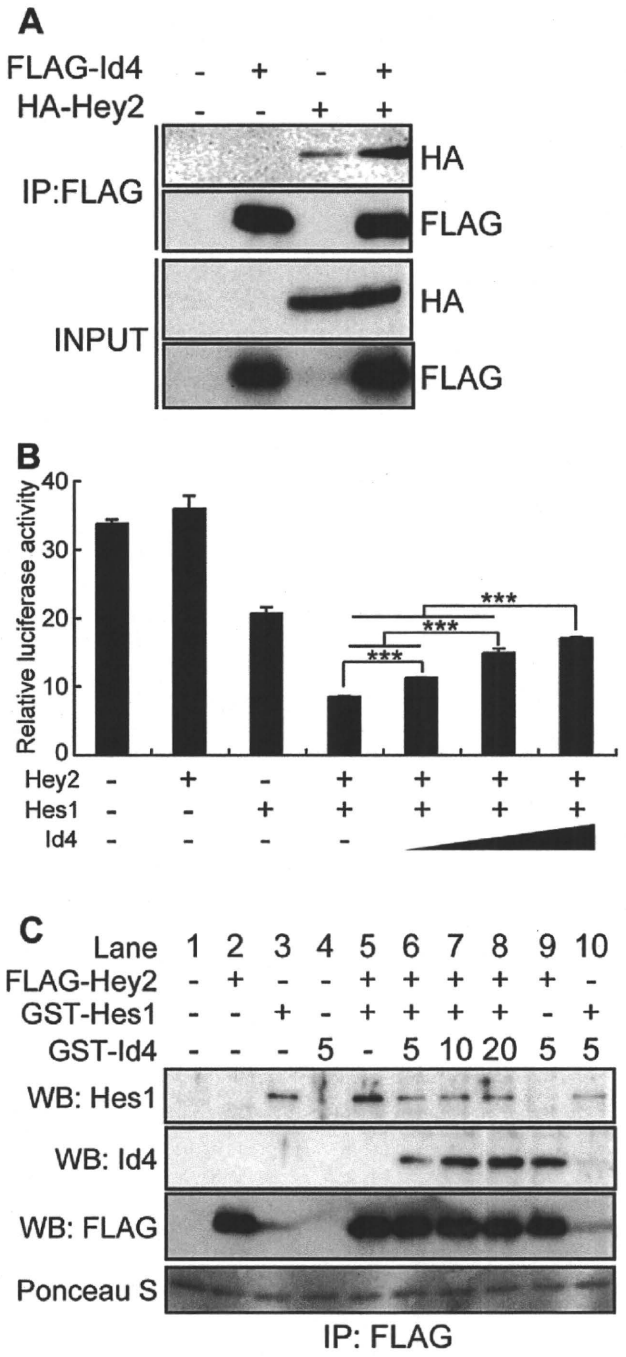

Figure 6. Id4 interacts with Hey2 and inhibits the suppression of reporter activity by Hey2/Hes1 complex. (A) Interaction of FLAG-tagged Id4 (FLAG-Id4) and human influenza hemagglutinin-tagged Hey2 (HA-Hey2) was confirmed in 293FT cells by immunoprecipitation (IP). (B) CV1 cells transfected with 6×E-box luciferase reporter, Hey2 and Hes1 expression vectors and with increasing doses of Id4 expression vector. Luciferase assay data were subjected to Student's t-tests. Each error bar represents the mean ± SE of triplicates. ***$p<0.005$ versus control. (C) *In vitro* assay of Id4 dose-dependent attenuation of Hey2-Hes1 complex interaction. GST-Id4 volume added was 5, 10 and 20 µl, respectively. WB: Western blotting.
doi:10.1371/journal.pgen.1001019.g006

osteoblasts were isolated from $Id4^{+/+}$ and $Id4^{-/-}$ neonatal calvarial bone as described previously [35]. Osteogenic differentiation was induced by changing the medium every three days to culture medium supplemented with 100 ng/ml of bone morphogenetic protein 4 (BMP4) (R&D Systems, Mineapolis, MN) and adipogenic differentiation was induced by changing the medium to differentiation medium supplemented with 10% fetal bovine serum (FBS), 0.5 mM 3-isobutyl-1-methlxanthine, 0.25 µM dexamethasone, and insulin-transferrin-selenium-X supplement containing 5 µg/ml of insulin (Invitrogen, Carlsbad, CA) and 1 µM rosiglitazone. After 48 hr, the differentiation medium was replaced with culture medium supplemented with 10% FBS.

Id4 knockdown by siRNA

siRNA sequences targeting the mouse Id4 transcript were purchased from Ambion (for adipocyte) and Invitrogen (for osteoblast). AllStar Negative Control siRNA (QIAGEN, cat. No., 1027281) and Negative Universal Control Med#2 (Invitrogen, cat. No., 12935-112) was used as a negative control in adipocyte and osteoblast differentiation, respectively. The sequences of siRNA used for Id4 knockdown were as follows; sense, CCUUUGUAUUUGACGUGUAtt; antisense, UACACGUCAAAUACAAAGGtt (Ambion, cat No. AM16704, ID. 159536); for adipocyte differentiation; sense, UUAAUUUCUGCUCUGGCCCUCCCUU; antisense, AAGGGAGGGCCAGAGCAGAAAUUAA (Invitrogen, stealth_455, cat No. 10620312); for osteoblast differentiation. For siRNA transfection, a complex of Lipofectamine 2000 (Invitrogen) and 20 nM siRNA was prepared according to the manufacturer's instruction and directly mixed with cells in the culture plates. The medium was replaced at 4–6 hr after transfection with fresh differentiation medium (adipogenic induction) or 10% FBS supplemented with 100 ng/ml of BMP4 (osteogenic induction).

Lipid assay and Alkaline phosphatase (ALP) staining

Lipid accumulation in adipocytes was detected by using Oil Red O staining as described previously [36]. The triglyceride content in adipocytes was determined as follows. ST2 cells were washed with cold phosphate-buffered saline (PBS) and total lipids were extracted with chloroform/methanol (2:1, v/v). The lower organic phase was dried, and the lipids were dissolved in 2-propanol. The triglyceride content was measured using Triglyceride E-test (Wako, Japan) according to the manufacturer's instructions. Protein concentrations were determined with Quick Start Bradford Dye Reagent (BIO RAD, 500-0205), using bovine gamma globulin as standard. ALP staining and measurements were performed as described previously [34].

Isolation of total RNA and quantitative real-time PCR (qRT–PCR)

Total RNA was isolated from liver, brain, kidney, thymus, brown adipose tissue (BAT), heart, white adipose tissue (WAT), adrenal gland, cortical bone, calvaria, bone marrow and posterior limb of E18.5 mouse embryo using TRIzol reagent (Invitrogen) and RNeasy columns (QIAGEN, Hilden, Germany) according to the manufacturer's instructions. Bone marrow was obtained by slicing of the ends of femur and tibia bones and then flushing it out with PBS using a syringe. Yield and quality of RNA were determined with a NanoDrop spectrometer (NanoDrop Technology, San Diego, CA) and a BioAnalyzer (Agilent Technologies, Santa Clara, CA). Gene expression levels were measured by qRT-PCR as described previously [34]. The sequences of forward and reverse primers used for each gene amplification were as follows; *gapdh*, GAPDH_768Fw_qPCR 5′-TGGAGAAACCTGCCAAGTATG-3′, GAPDH_889Rv_qPCR 5′-GGAGACAACCTGGTCCTCAG-3′; *Id4*, Mm_Id4_532Fw 5′-AGGGTGACAGCATTCTCTGC-3′, Mm_Id4_658Rv 5′-CCGGTGGCTTGTTTCTCTTA-3′; *Pparγ2*, PPARg2Fw 5′-ATGGGTGAAACTCTGG-

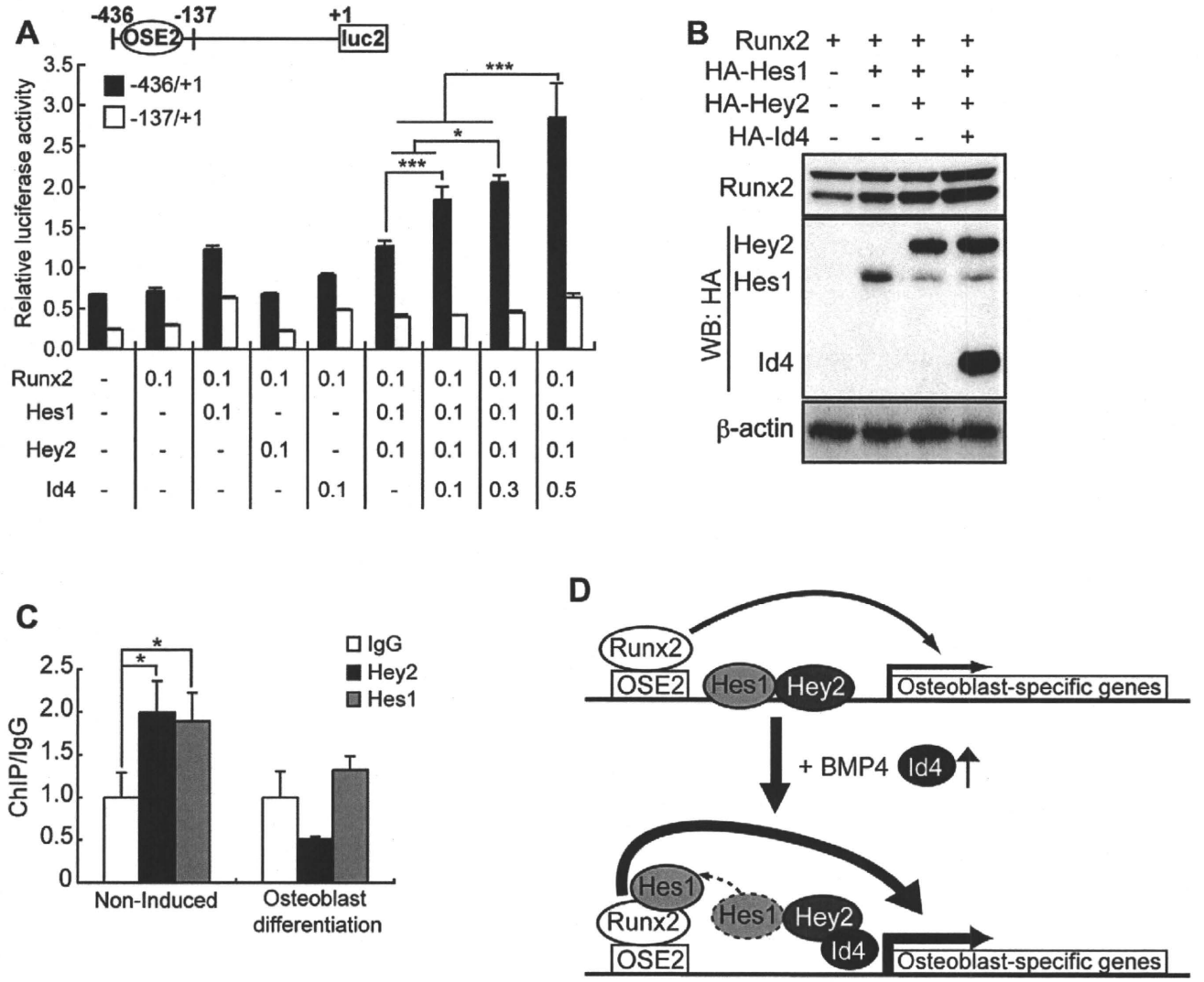

Figure 7. Id4 enhanced Runx2 transcriptional activity through stabilization of Runx2 protein. (A) Relative luciferase activity of *Bglap1* promoter in CV1 cells transfected with Runx2, Hes1, Hey2 and Id4 expression vectors. *Bglap1* promoter luciferase reporters were used as Runx2-dependent (−436bp/+1bp) or Runx2-independent (−137bp/+1bp). Luciferase assay data were subjected to Student's t-tests. Each error bar represents the mean ± SE of triplicates. *$p<0.05$ versus control and ***$p<0.005$ versus control. +1; transcription start site, bp; base pair. (B) Western blot analysis of Cos7 whole cell lysate using anti-Runx2, anti-HA and anti-β-actin (loading control) antibodies. The stability of Runx2-Hes1 complex increased in the presence of Id4. (C) ChIP-qPCR analyses of Hey2 and Hes1 binding onto *Bglap1* promoter in ST2 cells at day 4 after induction of osteoblast differentiation or non-induced ST2 cells. (D) A model of Id4 promoting Runx2-induced osteoblast differentiation.
doi:10.1371/journal.pgen.1001019.g007

GAGA-3′, PPARg2-1Rv 5′-GAGCTGATTCCGAAGTTGGT-3′; Bglap1, OC(PM15547142)Fw 5′-CTCTGTCTCTC TGAC-CTCACAG-3′, OC(PM15547142)Rv 5′-GGAGCTGCTGTGA-CATCCATAC-3′; *Adipoq*, Mm_AdipoQ_298Fw 5′-GATGG-CACTCCTGGAGAGAA-3′, Mm_AdipoQ_443Rv 5′-GCTTC-TCCAGGCTCTCCTTT-3′.

Expression microarray experiments

RNA was extracted from differentiating ST2 osteoblasts and adipocytes after induction of differentiation, using PureLink miRNA Isolation Kit (Invitrogen) according to the manufacture's instructions for total RNA purification. Total RNA derived from ST2 at 0 hr was used as control. Biotin-labeled cRNA was synthesized as recommended by Affymetrix guidelines. Labeled samples were hybridized to the Affymetrix GeneChip Mouse Genome 420 2.0 arrays according to the manufacturer's protocol. Scanning and intensity data analysis was preformed as described elsewhere [37].

Expression profiling analyses in ST2 osteoblast and adipocyte differentiation

Collected microarray expression data was background-subtracted, and normalized using the robust multi-array analysis method [37]. Differentially expressed genes were determined by selecting expression subgroups that contained the probe sets of up/down-regulated genes. Genes were considered up-regulated (down-regulated) if their $\log_2$ intensity ratio was greater (less) than 1 (−1), or greater (less) than the mean plus (minus) 3-times standard deviation. All gene and probe set annotations were derived from Ensembl release 52. Genes with transcription-related Gene Ontology (GO) annotations (Table 3) were considered as transcription factor-coding genes. Genes with

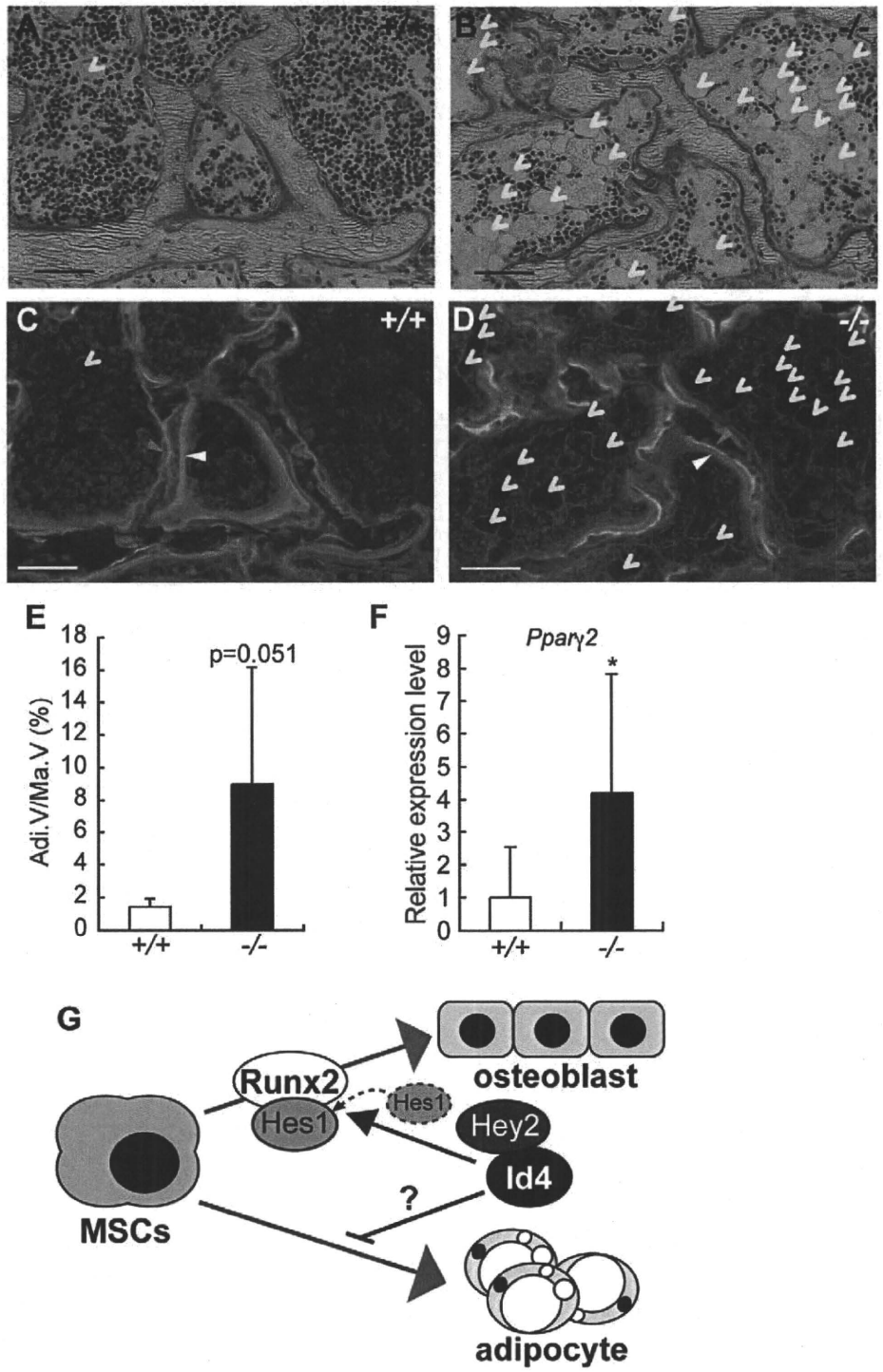

Figure 8. 4-week-old *Id4*$^{-/-}$ mice show increased adipocytes in bone marrow. (A,B) Villanueva staining of epiphyseal tibia of *Id4*$^{+/+}$ (A) and *Id4*$^{-/-}$ mice (B). (C,D) The BFR was measured in the tibial epiphysial regions in *Id4*$^{+/+}$ (C) and *Id4*$^{-/-}$ mice (D) using a fluorescence microscopy following double-staining with tetracycline hydrochloride (blue arrowheads) and calcein (white arrowheads). Yellow arrowheads indicate adipocytes. The original magnifications and scale bars of the images are ×400 and 100 μm. (E) The total area occupied by adipocytes (Adi.V) in the epiphyseal tibia bone marrow. *Id4*$^{+/+}$ (n = 6), *Id4*$^{-/-}$ (n = 6). (F) *Pparγ2* mRNA expression is significantly elevated in bone marrow cells of *Id4*$^{-/-}$ compared to *Id4*$^{+/+}$ mice. Relative expression levels of *Pparγ2* mRNA were measured by qRT-PCR. *Id4*$^{+/+}$ (n = 9), *Id4*$^{-/-}$ (n = 10). All data were subjected to Student's t-tests. Each error bar represents the mean ± SE. *$p<0.05$ versus control. (G) The role of Id4 in bone formation and bone marrow environment.
doi:10.1371/journal.pgen.1001019.g008

InterPro accession IPR001092 were annotated as bHLH transcription factor-coding genes. Spotfire DecisionSite version 8.1.1 (TIBCO Software, Inc.) was used for hierarchical clustering and generating the gene expression heat maps.

Luciferase reporter assays

Bglap1 promoter regions were cloned by PCR from the mouse genome. 6×E-box sequence (CGCGTCCACGTGGGGCCAC-GTGGGGCCACGTGGGGCCACGTGGG GCCACGTGGG-

Table 3. Gene ontology IDs and terms (GO release 2009-01-25) associated with 1,270 transcription factors of Table 1.

GO ID	GO Term
GO:0000156	two-component response regulator activity
GO:0003700	transcription factor activity
GO:0003701	RNA polymerase I transcription factor activity
GO:0003702	RNA polymerase II transcription factor activity
GO:0003704	specific RNA polymerase II transcription factor activity
GO:0003705	RNA polymerase II transcription factor activity, enhancer binding
GO:0003706	ligand-regulated transcription factor activity
GO:0003709	RNA polymerase III transcription factor activity
GO:0003711	transcription elongation regulator activity
GO:0003712	transcription cofactor activity
GO:0003713	transcription coactivator activity
GO:0003714	transcription corepressor activity
GO:0003715	transcription termination factor activity
GO:0003716	RNA polymerase I transcription termination factor activity
GO:0003717	RNA polymerase II transcription termination factor activity
GO:0003718	RNA polymerase III transcription termination factor activity
GO:0008140	cAMP response element binding protein binding
GO:0008148	negative transcription elongation factor activity
GO:0008159	positive transcription elongation factor activity
GO:0016251	general RNA polymerase II transcription factor activity
GO:0016252	nonspecific RNA polymerase II transcription factor activity
GO:0016455	RNA polymerase II transcription mediator activity
GO:0016563	transcription activator activity
GO:0016564	transcription repressor activity
GO:0016565	general transcriptional repressor activity
GO:0016566	specific transcriptional repressor activity
GO:0016943	RNA polymerase I transcription elongation factor activity
GO:0016944	RNA polymerase II transcription elongation factor activity
GO:0016945	RNA polymerase III transcription elongation factor activity
GO:0016986	transcription initiation factor activity
GO:0016987	sigma factor activity
GO:0016988	transcription initiation factor antagonist activity
GO:0016989	sigma factor antagonist activity
GO:0017163	negative regulator of basal transcription activity
GO:0030374	ligand-dependent nuclear receptor transcription coactivator activity
GO:0030375	thyroid hormone receptor coactivator activity
GO:0030401	transcription antiterminator activity
GO:0030528	transcription regulator activity
GO:0042156	zinc-mediated transcriptional activator activity

doi:10.1371/journal.pgen.1001019.t003

GCCACGTGGGGA) and cloned fragments were ligated to the firefly luciferase gene (derived from pGL4.10, Promega). CV1 cells were co-transfected with the firefly luciferase reporter vectors, expression vectors and the internal control Renilla luciferase vector (pGL4.74, Promega) using Lipofectamine 2000 (Invitrogen). Luciferase activities were measured with Wallac 1420 Multilabel counter (PerkinElmer Life and Analytical Sciences, Turku, Finland). These experiments were performed in triplicate.

Co-immunoprecipitation and GST–pull down assay

Cos7 cells were transfected with FLAG-Id4 expression vector with either HA tagged expression vector (Hes1, Hey1, Hey2, Bhlhe40). The extracts from the transfected cells were incubated with Protein G sepharose beads and precipitated with either anti-FLAG antibody (SIGMA) or normal mouse IgG (Santa cruz) overnight at 4C°. After washing with PBS, bound proteins were separated by SDS-PAGE followed by Western blot analysis with anti-HA antibody, anti-FLAG antibody. GST-Id4 expression vector, Flag-Hey2 expression vector and Flag-empty vector were expressed in *E.coli*. The crude extract of GST-Id4 or GST expressed in *E.coli* was incubated with glutatihione sepharose beads for 4 hr at 4C°. The precipitate was incubated with the extract of Flag-Hey2 overnight at 4C°. After washing, the bound proteins were separated by SDS-PAGE followed by Western blot analysis with anti-Flag antibody.

Chromatin Immunoprecipitation (ChIP)–qPCR analysis

ChIP was performed as described previously [38]. ST2 cells were cultured for 4 days with or without 100 ng/ml BMP4, respectively. The antibodies used for ChIP were anti-Hey2 (Protein Tech Group, cat No. 10597-1-AP), anti-Hes1 (Santa Cruz, H-140) and normal rabbit IgG (Santa Cruz, sc-2027) as negative control. Forward and reverse qPCR primer sequences contained OSE2 of the *Bglap1* promoter (Bglap2_ChIP_L789, 5′-GATTGTGGCCTCTCGTC-3′;Bglap2_ChIP_R8, 5′- ATCG-GCTACTCTGTGCTCT-3′).

Animals

Id4$^{-/-}$ mice previously generated by Bedford et al. (2005) were kindly supplied by Dr. Kondo who received them originally from Dr. Sablitzky (University of Nottingham). All mice used in this study were maintained and handled according to the protocols approved by the Animal Research Committee of Saitama Medical University.

Bone morphometric measurements

To assess the static and dynamic parameters of bone histomorphometry, 3 weeks old female mice were labeled with intraperitoneal injections of 20 mg/kg of tetracycline hydrochloride (Sigma) at 4 days before sacrifice. Two days before sacrifice, the mice were injected with 10 mg/kg of calcein (Dojindo Co., Kumamoto, Japan). Tibiae and lumbar vertebrae were removed from each mouse, and fixated with 70% ethanol. The bones were trimmed to remove the muscle, stained with Villanueva bone stain for 5 days, dehydrated in graded concentrations of ethanol, and embedded in methyl-methacrylate (Wako Chemicals, Kanagawa, Japan) without decalcification. Sagittal plane sections (5 μm thick) of the lumbar vertebrae were cut using a Microtome (Leica, Germany). Bone morphometric analyses were performed using a semi-automatic image analyzing system software (System Supply, Nagano, Japan) and Optiphot fluorescent microscope (Nikon, Tokyo, Japan).

Supporting Information

Figure S1 Heat-map of osteoblast differentiation phase-specific up-regulated transcription factor genes. Transcription factors of the bHLH family are indicated by purple bars. The column 'Cluster groups' shows the gene symbols of up-regulated transcription factors in time-sequential (chronological) cluster order. The gene symbols of the up-regulated transcription factors are listed in the same order as they appear on the image. Phase 1 (1hr; 46 transcription factors): Foxc2, Nfatc1, Hoxb2, Fkhl18,

Med14, Id4, Msx2, Id2, Ankrd1, Hes1, Bhlhe40, Foxn1, Tle4, Hmga2, Dlx3, Gata2, Dlx2, Nr4a3, Axud1, Eaf1, Hipk2, AC153948.5, Zfx, Cebpb, Grhl1, Smad7, Rel, Maff, Mafk, Klf16, Id1, Nfil3, Fosl1, Klf5, Npas4, Lmcd1, Atf3, Fosb, Mef2c, Erf, Mef2a, Atp6v0a1, Srf, Tgif1, Nr4a1 and Junb; phase 2 (6–24hr; 29 transcription factors); Hey1, Atoh8, Helb, Hdac9, Atf6, Gcom1, Hoxa1, Prrx1, Tgfb1, Creb3l1, Rbm9, Elk3, C1d, Dlx1, Pde8a, Hey2, Ets2, Dtna, Smad6, Foxo1, Cux1, Gatad2b, Irf5, Rfc1, Sp7, Arnt2, Aebp1, Hoxc13 and Aff3; phase 3 (30–48hr; 4 transcription factors): Lef1, Fabp4, Stat5a, Prrx2; phase 4 (4–6d; 7 transcription factors): Hod, Maf, Foxf2, Sox9, Stat1, Foxd1 and Neo1; phase 5 (8–14d; 24 transcription factors): Stat2, Esr1, Klf9, Klf13, AC162313.5, Cml3, Pou6f1, Pura, Nfat5, Zfp521, Trib3, Ddit3, 2210012G02Rik, Clock, Irf7, Nr3c1, Irf9, Zhx2, Sqstm1, Znfx1, Atf5, Hoxa9, Nr1d2 and Nfe2l1.
Found at: doi:10.1371/journal.pgen.1001019.s001 (1.10 MB TIF)

Figure S2 *Id4* expression pattern in ST2 osteoblast (A) and adipocyte (B) differentiation. Relative expression levels of *Id4* mRNA were measured by qRT-PCR.
Found at: doi:10.1371/journal.pgen.1001019.s002 (0.16 MB TIF)

Figure S3 4-week-old $Id4^{-/-}$ mice show decrease of growth plate in tibia. (A,B) Villanueva staining of growth plate of $Id4^{+/+}$ (A) and $Id4^{-/-}$ (B) mice tibia. The original magnifications and scale bars of the images are ×64 and 500 μm. (C) Growth plate width in tibia. (D) Longitudinal Growth Rate (Lo. G. R) in tibia. All data were subjected to Student's t-tests. $^{***}p<0.005$ versus control. Each error bar represents the mean±SE of $Id4^{+/+}$ (n = 6) and $Id4^{-/-}$ (n = 6), respectively.
Found at: doi:10.1371/journal.pgen.1001019.s003 (2.67 MB TIF)

Figure S4 Id4 associates with Hey2. (A) Isolation of bHLH transcription factors binding with Id4 was performed by immunoprecipitation (IP). IP was carried out using anti-FLAG antibody and Western blot analysis (WB) was performed using anti-HA antibody. Arrowheads indicate that Hey2 binds with Id4. (B) Direct interaction of recombinant glutathione S-transferase-tagged Id4 (GST-Id4) and recombinant FLAG-tagged Hey2 (FLAG-Hey2) was confirmed *in vitro*. The GST-pull down assay performed using glutathione sepharose beads bound to recombinant GST-Id4. Recombinant FLAG-Hey2 was detected with anti-FLAG antibody.
Found at: doi:10.1371/journal.pgen.1001019.s004 (0.22 MB TIF)

Figure S5 Expression level of osteoblast marker *in vivo*. (A) Ratio of relative *Bglap1* mRNA expression level between osteoblast-induced POB and non-induced POB from $Id4^{+/+}$ and $Id4^{-/-}$ neonatal calvarial bone. $Id4^{+/+}$ (n = 37), $Id4^{-/-}$ (n = 21). qRT-PCR data were subjected to Student's t-tests. $^{**}p<0.01$ versus control. (B) Relative expression levels of *Id4* and *Bglap1* mRNA in $Id4^{+/+}$ and $Id4^{-/-}$ mouse embryo (E18.5) posterior limb were measured by qRT-PCR. $Id4^{+/+}$ (n = 1), $Id4^{-/-}$ (n = 4). Each error bar represents the mean±SE of triplicates.
Found at: doi:10.1371/journal.pgen.1001019.s005 (0.18 MB TIF)

Table S1 List of transcription factors expressed in induced ST2 cells differentiating into osteoblasts or adipocytes. Bhlh members are indicated using bold type. Arrows indicate up- (↑), down-regulated (↓), or up- and down-regulated (↑ ↓) transcription factors. No change in expression levels is symbolized by the almost equal sign (≈).
Found at: doi:10.1371/journal.pgen.1001019.s006 (0.10 MB XLS)

Acknowledgments

We greatly appreciate the technical assistance of M. Iseki, S. Okumura, M. Kitazato, M. Otsu, and K. Tanaka. We are grateful to K. Kano, M. Kohda, A. Itoh, H. Asahara, Y. Ito, and H. Iseki for their thoughtful discussion. We thank Y. Hayashizaki, J. Kawai, and H. Suzuki for critical suggestions and supporting the project.

Author Contributions

Conceived and designed the experiments: Y Tokuzawa, K Yagi, Y Mizuno, Y Okazaki. Performed the experiments: Y Tokuzawa, K Yagi, Y Yamashita, Y Ninomiya, Y Kanesaki-Yatsuka, M Akita, H Motegi, S Wakana, T Noda, Y Mizuno. Analyzed the data: Y Tokuzawa, Y Yamashita, Y Nakachi, I Nikaido, H Bono. Contributed reagents/materials/analysis tools: F Sablitzky, S Arai, R Kurokawa, T Fukuda, T Katagiri. Wrote the paper: Y Tokuzawa, K Yagi, Y Nakachi, C Schönbach, T Suda, Y Okazaki.

References

1. Burkhardt R, Kettner G, Bohm W, Schmidmeier M, Schlag R, et al. (1987) Changes in trabecular bone, hematopoiesis and bone marrow vessels in aplastic anemia, primary osteoporosis, and old age: a comparative histomorphometric study. Bone 8: 157–164.
2. Nuttall ME, Gimble JM (2004) Controlling the balance between osteoblastogenesis and adipogenesis and the consequent therapeutic implications. Curr Opin Pharmacol 4: 290–294.
3. Akune T, Ohba S, Kamekura S, Yamaguchi M, Chung UI, et al. (2004) PPARgamma insufficiency enhances osteogenesis through osteoblast formation from bone marrow progenitors. J Clin Invest 113: 846–855.
4. Kobayashi H, Gao Y, Ueta C, Yamaguchi A, Komori T (2000) Multilineage differentiation of Cbfa1-deficient calvarial cells in vitro. Biochem Biophys Res Commun 273: 630–636.
5. Lian JB, Stein GS, Javed A, van Wijnen AJ, Stein JL, et al. (2006) Networks and hubs for the transcriptional control of osteoblastogenesis. Rev Endocr Metab Disord 7: 1–16.
6. Nishimura R, Hata K, Ikeda F, Ichida F, Shimoyama A, et al. (2008) Signal transduction and transcriptional regulation during mesenchymal cell differentiation. J Bone Miner Metab 26: 203–212.
7. Takada I, Mihara M, Suzawa M, Ohtake F, Kobayashi S, et al. (2007) A histone lysine methyltransferase activated by non-canonical Wnt signalling suppresses PPAR-gamma transactivation. Nat Cell Biol 9: 1273–1285.
8. Iwata T, Kawamoto T, Sasabe E, Miyazaki K, Fujimoto K, et al. (2006) Effects of overexpression of basic helix-loop-helix transcription factor Dec1 on osteogenic and adipogenic differentiation of mesenchymal stem cells. Eur J Cell Biol 85: 423–431.
9. Buskin JN, Hauschka SD (1989) Identification of a myocyte nuclear factor that binds to the muscle-specific enhancer of the mouse muscle creatine kinase gene. Mol Cell Biol 9: 2627–2640.
10. Arnold HH, Braun T (1996) Targeted inactivation of myogenic factor genes reveals their role during mouse myogenesis: a review. Int J Dev Biol 40: 345–353.
11. Kim JB, Spiegelman BM (1996) ADD1/SREBP1 promotes adipocyte differentiation and gene expression linked to fatty acid metabolism. Genes Dev 10: 1096–1107.
12. Ross SE, Greenberg ME, Stiles CD (2003) Basic helix-loop-helix factors in cortical development. Neuron 39: 13–25.
13. Ross DA, Hannenhalli S, Tobias JW, Cooch N, Shiekhattar R, et al. (2006) Functional analysis of Hes-1 in preadipocytes. Mol Endocrinol 20: 698–705.
14. Lee JS, Thomas DM, Gutierrez G, Carty SA, Yanagawa S, et al. (2006) HES1 cooperates with pRb to activate RUNX2-dependent transcription. J Bone Miner Res 21: 921–933.
15. Tontonoz P, Hu E, Graves RA, Budavari AI, Spiegelman BM (1994) mPPAR gamma 2: tissue-specific regulator of an adipocyte enhancer. Genes Dev 8: 1224–1234.
16. Hu E, Liang P, Spiegelman BM (1996) AdipoQ is a novel adipose-specific gene dysregulated in obesity. J Biol Chem 271: 10697–10703.
17. Bedford L, Walker R, Kondo T, van Cruchten I, King ER, et al. (2005) Id4 is required for the correct timing of neural differentiation. Dev Biol 280: 386–395.
18. Sun XH, Copeland NG, Jenkins NA, Baltimore D (1991) Id proteins Id1 and Id2 selectively inhibit DNA binding by one class of helix-loop-helix proteins. Mol Cell Biol 11: 5603–5611.
19. Iso T, Sartorelli V, Poizat C, Iezzi S, Wu HY, et al. (2001) HERP, a novel heterodimer partner of HES/E(spl) in Notch signaling. Mol Cell Biol 21: 6080–6089.
20. Komori T, Yagi H, Nomura S, Yamaguchi A, Sasaki K, et al. (1997) Targeted disruption of Cbfa1 results in a complete lack of bone formation owing to maturational arrest of osteoblasts. Cell 89: 755–764.

21. Otto F, Thornell AP, Crompton T, Denzel A, Gilmour KC, et al. (1997) Cbfa1, a candidate gene for cleidocranial dysplasia syndrome, is essential for osteoblast differentiation and bone development. Cell 89: 765–771.
22. Nakashima K, Zhou X, Kunkel G, Zhang Z, Deng JM, et al. (2002) The novel zinc finger-containing transcription factor osterix is required for osteoblast differentiation and bone formation. Cell 108: 17–29.
23. Ducy P, Karsenty G (1995) Two distinct osteoblast-specific cis-acting elements control expression of a mouse osteocalcin gene. Mol Cell Biol 15: 1858–1869.
24. Suh JH, Lee HW, Lee JW, Kim JB (2008) Hes1 stimulates transcriptional activity of Runx2 by increasing protein stabilization during osteoblast differentiation. Biochem Biophys Res Commun 367: 97–102.
25. Kulterer B, Friedl G, Jandrositz A, Sanchez-Cabo F, Prokesch A, et al. (2007) Gene expression profiling of human mesenchymal stem cells derived from bone marrow during expansion and osteoblast differentiation. BMC Genomics 8: 70.
26. Liu T, Gao Y, Sakamoto K, Minamizato T, Furukawa K, et al. (2007) BMP-2 promotes differentiation of osteoblasts and chondroblasts in Runx2-deficient cell lines. J Cell Physiol 211: 728–735.
27. Sciaudone M, Gazzerro E, Priest L, Delany AM, Canalis E (2003) Notch 1 impairs osteoblastic cell differentiation. Endocrinology 144: 5631–5639.
28. Nobta M, Tsukazaki T, Shibata Y, Xin C, Moriishi T, et al. (2005) Critical regulation of bone morphogenetic protein-induced osteoblastic differentiation by Delta1/Jagged1-activated Notch1 signaling. J Biol Chem 280: 15842–15848.
29. Maeda Y, Tsuji K, Nifuji A, Noda M (2004) Inhibitory helix-loop-helix transcription factors Id1/Id3 promote bone formation in vivo. J Cell Biochem 93: 337–344.
30. Katagiri T, Imada M, Yanai T, Suda T, Takahashi N, et al. (2002) Identification of a BMP-responsive element in Id1, the gene for inhibition of myogenesis. Genes Cells 7: 949–960.
31. Lopez-Rovira T, Chalaux E, Massague J, Rosa JL, Ventura F (2002) Direct binding of Smad1 and Smad4 to two distinct motifs mediates bone morphogenetic protein-specific transcriptional activation of Id1 gene. J Biol Chem 277: 3176–3185.
32. Zhang Y, Hassan MQ, Li ZY, Stein JL, Lian JB, et al. (2008) Intricate gene regulatory networks of helix-loop-helix (HLH) proteins support regulation of bone-tissue related genes during osteoblast differentiation. J Cell Biochem 105: 487–496.
33. Wan Y, Chong LW, Evans RM (2007) PPAR-gamma regulates osteoclastogenesis in mice. Nat Med 13: 1496–1503.
34. Mizuno Y, Yagi K, Tokuzawa Y, Kanesaki-Yatsuka Y, Suda T, et al. (2008) miR-125b inhibits osteoblastic differentiation by down-regulation of cell proliferation. Biochem Biophys Res Commun 368: 267–272.
35. Yang S, Takahashi N, Yamashita T, Sato N, Takahashi M, et al. (2005) Muramyl dipeptide enhances osteoclast formation induced by lipopolysaccharide, IL-1 alpha, and TNF-alpha through nucleotide-binding oligomerization domain 2-mediated signaling in osteoblasts. J Immunol 175: 1956–1964.
36. Yagi K, Kondo D, Okazaki Y, Kano K (2004) A novel preadipocyte cell line established from mouse adult mature adipocytes. Biochem Biophys Res Commun 321: 967–974.
37. Irizarry RA, Bolstad BM, Collin F, Cope LM, Hobbs B, et al. (2003) Summaries of Affymetrix GeneChip probe level data. Nucleic Acids Res 31: e15.
38. Wakabayashi K, Okamura M, Tsutsumi S, Nishikawa NS, Tanaka T, et al. (2009) The peroxisome proliferator-activated receptor gamma/retinoid X receptor alpha heterodimer targets the histone modification enzyme PR-Set7/Setd8 gene and regulates adipogenesis through a positive feedback loop. Mol Cell Biol 29: 3544–3555.

Cancer Science
The official journal of the Japanese Cancer Association

Human Arm protein lost in epithelial cancers, on chromosome X 1 (*ALEX1*) gene is transcriptionally regulated by CREB and Wnt/β-catenin signaling

Hiroyoshi Iseki,[1,3] Akihiko Takeda,[1,3,6,7] Toshiwo Andoh,[2,3] Norio Takahashi,[3] Igor V. Kurochkin,[4] Aliaksandr Yarmishyn,[4] Hideaki Shimada,[5,9] Yasushi Okazaki[2,8] and Isamu Koyama[1,3,8]

[1]Department of Digestive Surgery, [2]Division of Functional Genomics and Systems Medicine, and [3]Project Research Division, Research Center for Genomic Medicine, Saitama Medical University, Saitama, Japan; [4]Genome and Gene Expression Data Analysis Division, Bioinformatics Institute, Matrix, Singapore; [5]Department of Digestive Surgery, Chiba Cancer Center, Chiba, Japan; [6]Department of Digestive Surgery, International University of Health and Welfare Hospital, Tochigi, Japan

(Received September 15, 2009/Revised January 29, 2010/Accepted February 3, 2010/Accepted manuscript online March 24, 2010/Article first published online April 20, 2010)

The aberrant activation of Wnt signaling is a key process in colorectal tumorigenesis. Canonical Wnt signaling controls transcription of target genes via β-catenin and T-cell factor/lymphoid enhancer factor family transcription factor complex. Arm protein lost in epithelial cancers, on chromosome X 1 (*ALEX1*) is a novel member of the Armadillo family which has two Armadillo repeats as opposed to more than six repeats in the classical Armadillo family members. Here we examine *cis*-regulatory elements and *trans*-acting factors involved in the transcriptional regulation of the *ALEX1* gene. Site-directed mutations of a cyclic AMP response element (CRE) and an E-box impaired the basal activity of human *ALEX1* promoter in colorectal and pancreatic cancer cell lines. Moreover, overexpression of CRE-binding protein (CREB) increased the *ALEX1* promoter activity in these cell lines, whereas knockdown of *CREB* expression decreased the expression level of *ALEX1* mRNA. Interestingly, luciferase reporter analysis and quantitative real-time RT-PCR demonstrated that the *ALEX1* promoter was up-regulated in a CRE-dependent manner by continuous activation of Wnt/β-catenin signaling induced by a glycogen synthase kinase-3 inhibitor and overexpression of β-catenin. These results indicate that the CRE and E-box sites are essential *cis*-regulatory elements for *ALEX1* promoter activity, and *ALEX1* expression is regulated by CREB and Wntk/β-catenin signaling. (*Cancer Sci* 2010; 101: 1361–1366)

Wnt signaling is important for embryonic development, stem cell maintenance, and tumorigenesis.[1,2] Two Armadillo (Arm) family members, β-catenin and adenomatous polyposis coli (APC), are essential components of the Wnt signaling pathway. β-Catenin is mainly localized to the plasma membrane in normal colon mucosa, whereas the cytoplasmic β-catenin is phosphorylated by the degradation complex composed of casein kinase I, glycogen synthase kinase-3β (GSK-3β), APC, and AXIN, and subsequently degraded by the ubiquitin–proteasome pathway. In over 80% of colorectal cancers, β-catenin aberrantly accumulates in the cytoplasmic and nuclear regions due to inactivating mutations in APC, forming a complex with the T-cell factor/lymphoid enhancer factor (TCF/LEF) family of transcription factors, leading to activation of the Wnt signaling pathway.[3,4] To elucidate the role of the Wnt signaling in tumor development and stem cell maintenance, numerous candidate target genes of the β-catenin/TCF have been identified.[5–7]

The cyclic AMP response element (*CRE*)-binding protein/activating transcription factor (*CREB/ATF*) belongs to the basic region/leucine zipper transcription factor family.[8] Traditionally, it has been believed that CREB dimers bind to CRE sites under basal conditions, but they are inactive; and that activation of CREB is mediated by phosphorylation at a specific serine residue. This phosphorylation promotes the association of CREB with the transcriptional co-activator CREB-binding protein and its paralogue p300, leading to activation of its target genes through histone modification and recruitment of an active transcription complex.[8] It is noteworthy that CREB synergistically or predominantly activates some of its target genes through β-catenin via CRE sites.[9–11]

Arm protein lost in epithelial cancers, on chromosome X (*ALEX*; also known as Armadillo repeat containing, X-linked [*ARMCX*]) is a novel member of the Arm family which has one or two Arm repeats as opposed to more than six repeats in the classical Arm family members.[12] The *ALEX* family, consisting of at least three variants (*ALEX1*, *ALEX2*, and *ALEX3*), is closely localized on chromosome Xq21.33–q22.2.[12] Human *ALEX1* is composed of four exons with the coding region residing entirely in a single exon and encodes a predicted protein of 453 amino acids which is highly conserved between humans and mice (95% amino acid similarity).[13] *ALEX1* mRNA is widely expressed in human tissues but is dramatically reduced or even undetectable in several human carcinoma cell lines and tissues, suggesting that ALEX1 may play a role as a tumor suppressor.[12] However, the regulatory mechanism of the *ALEX1* gene in normal and cancer cells remains largely unknown. Here we examined the transcriptional regulation of the *ALEX1* gene in human cancer cell lines and found that *ALEX1* expression is regulated by CREB and Wnt/β-catenin signaling.

Materials and Methods

Cells and culture conditions. Human colon cancer cell lines HCT116 and SW480 were obtained from DS Pharma Biomedical (Osaka, Japan) and the Cell Resource Center for Biomedical Research, Tohoku University (Sendai, Japan), respectively. Human pancreatic cancer cell line PANC-1 was provided by the RIKEN Cell Bank (Tsukuba, Japan). HCT116 and SW480 cells were cultured in DMEM (Invitrogen, Tokyo, Japan) and PANC-1 cells were cultured in RPMI-1640 (Invitrogen) supplemented with 10% heat-inactivated FBS (Invitrogen) in a 5% CO_2 atmosphere at 37°C.

Plasmid constructs and transfection. The putative promoter region of the human *ALEX1* gene from −1933 to +487 was amplified by PCR and subcloned into the pCR-Blunt II-TOPO

[7]To whom correspondence should be addressed. E-mail: aktake@iuhw.ac.jp
[8]These authors equally contributed to this project in financial support.
[9]Present address: Department of Surgery, School of Medicine, Toho University, 6-11-1, Omorinishi, Ota-ku, Tokyo 143-8541, Japan.

doi: 10.1111/j.1349-7006.2010.01541.x

plasmid (Invitrogen). An approximately 2400-bp DNA fragment containing the *ALEX1* promoter sequence was inserted into the *Eco*RV and *Hin*dIII site of the pGL4.10 plasmid (Promega, Tokyo, Japan). The luciferase reporter plasmids driven by deleted mutant types of *ALEX1* promoter were generated by the same PCR-based method. Point mutations at potential TCF/LEF-binding element (TBE(s)), CRE, and E-box sites were introduced by PCR-based site-directed mutagenesis with PrimeSTAR polymerase (Takara Bio, Shiga, Japan).

Full-length open reading frames for human *ALEX1* and *CTNNB1* genes (accession nos NM_016608 and NM_001904, respectively) were amplified by PCR and inserted into the *Xho*I site of pCAGIPuro plasmid (kindly provided by Dr. H. Niwa, RIKEN), designated as pCAGIPuro/ALEX1 and pCAGIPuro/β-catenin, respectively. The plasmid containing the complete sequence of human *ALEX1* gene and the cDNA derived from HCT116 cells which expresses both wild-type and Ser^{45}-deleted β-catenin were used as templates for the amplification of *ALEX1* and *CTNNB1* genes, respectively.[12] The pCAGIPuro/EGFP plasmid (kindly provided by Dr. H. Niwa, RIKEN) encoding enhanced green fluorescence protein (EGFP) was used as a control.

Human *TCF4* (also known as *TCF7L2*), *ΔN-TCF4*, and *CREB* (*CREBΔ* isoform; accession no. NM 004379) genes were amplified by PCR and inserted into the *Eco*RI site of pCAGIPuro plasmid. Two dominant-negative mutants of the *CREBΔ* gene, $CREB^{R287L}$ (KCREB) and $CREB^{S119A}$ (CREBM1 and mCREB) in which Arg^{287} and Ser^{119} is converted to Leu and Ala, respectively, were generated by PCR-based site-directed mutagenesis.

Plasmid transfections were performed by Lipofectamine 2000 or Lipofectamine LTX (Invitrogen) according to the manufacturer's instructions. Primer sequences used for cloning and mutagenesis are available in Table S1 (Supporting information).

Luciferase reporter assay. The luciferase reporter assay was performed using the Dual-Glo Luciferase Assay System (Promega) according to the manufacturer's instructions. A total of 5000 cells were plated in a 96-well plate. After overnight culture, cells were transfected with 100 ng of the expression plasmid of Firefly reporter gene driven by human *ALEX1* promoter and 50 ng of Renilla luciferase control plasmid (pGL4.74; Promega) using Lipofectamine LTX and cultured for 48 h. TOPflash and FOPflash reporter plasmids (Millipore, Tokyo, Japan), which contain six wild-type and six mutated TBE sites, respectively, were used to evaluate β-catenin/TCF-dependent transcriptional activity. To activate Wnt/β-catenin signaling, cells were treated for 48 h with 6-bromoindirubin-3′-oxime (BIO) (Merck, Tokyo, Japan), at a final concentration of 5 μM, 4 h post transfection. As a control, the cells were treated with deionized distilled water and 5 μM 1-mehyl-6-bromoindirubin-3′-oxime (MeBIO) (Merck), respectively. Firefly and Renilla luciferases were measured by using the 1420 Multilabel Counter ARVO MX. The experiment was performed in triplicate and repeated at least three times.

Quantitative real-time RT-PCR. Total RNA was extracted by RNeasy mini kit (Qiagen, Tokyo, Japan) according to the manufacturer's instructions. First-strand cDNA was synthesized from 1 μg of total RNA using Transcriptor Reverse Transcriptase (Roche Diagnostics, Tokyo, Japan) in a total volume of 20-μL reaction mixtures. Quantitative real-time RT-PCR was performed using the Power SYBR Green PCR Master Mix (Applied Biosystems, Tokyo, Japan) and the MX3000P Real-time PCR System (Stratagene, La Jolla, CA, USA) according to the manufacturers' instructions. Primer sequences are available in Table S1 (Supporting information).

siRNA transfection. PANC-1 cells were transfected with the ON-TARGETplus Non-Targeting Control siRNA or siRNAs targeting CREB using DharmaFECT1 siRNA Transfection Reagent (Thermo Fisher Scientific, Lafayette, CO, USA), and cultured for 48 h. Quantitative real-time RT-PCR was performed using the Rotor-Gene SYBR Green PCR kit (Qiagen) and the Rotor-Gene Q PCR system (Qiagen). The following two ON-TARGETplus siRNAs targeting CREB were used: siRNA1, GAGAGAGGUCCGUCUAAUG; and siRNA2, GCCCAGCCAUCAGUUAUUC.

Chromatin immunoprecipitation (ChIP). ChIP assay was carried out in accordance with a previous report with several modification.[10] Immunoprecipitation was carried out with Dynabeads Protein G (Invitrogen) and polyclonal anti-CREB antibody (#9197; Cell Singling Technology, Danvers, MA, USA). The primer pair used to amplify *ALEX1* and cyclin D1 promoter sequences containing the putative CRE, and *ALEX1* 3′-distal region sequence were as follows: *ALEX1* promoter, 5′-GCTGCTGATGGGAGTGGTA-3′ and 5′-CGGACCAAACGAAGACTAGG-3′; cyclin D1 promoter, 5′-CTCCCGCTCCCATTCTCT-3′ and 5′-ACTCTGCTGCTCGCTGCTAC-3′; and *ALEX1* 3′-distal, 5′-ATGTGCAGCATGAGTCCAAG-3′ and 5′-ATTCCCATGGCCACCAGTA-3′.

Indirect immunofluorescence. The cells were washed in PBS, fixed in 100% methanol at −20°C for 5 min and in 4% paraformaldehyde in PBS at room temperature for 30 min, and permeabilized with 0.2% Triton X-100 in PBS at room temperature for 15 min. Permeabilized cells were washed three times with PBS, treated with 3% bovine serum albumin in PBS for 30 min, followed by incubation with antihuman β-catenin antibody at 1:250 dilution at room temperature for 1 h. After washing three times in PBS, the cells were incubated with Rhodamine-conjugated antimouse IgG antibody (Chemicon) at 1:100 in PBS at room temperature for 1 h. Finally, the cells were mounted in Vectashield Mounting Medium with DAPI (4′,6′-diamidino-2-phenylindole; Vector Laboratories, Burlingame, CA, USA). The images were obtained using a Axiovert 200M fluorescent microscope (Carl Zeiss MicroImaging, Tokyo, Japan).

Statistical analysis. Statistics were performed using the Mann–Whitney *U*-test for the expression analysis and luciferase reporter assay. A *P*-value less than 0.05 was considered to be statistically significant.

Nucleotide sequence accession numbers. The sequences of human *TCF4* gene and human *ALEX1* promoter cloned in this study have been deposited in the DDBJ/EMBL/GenBank databases under accession numbers AB440195 and AB440194, respectively.

Results

CREB regulates human *ALEX1* promoter activity. To identify candidates for *cis*-regulatory elements involved in the regulation of *ALEX1* gene expression, we carried out a computational search for transcription factor binding sites, and found a CREB/ATF binding site, CRE, and a basic helix-loop-helix transcription factors-binding site, E-box, at the proximal region of the transcription start site of human *ALEX1* gene (Fig. 1a), which are highly conserved between humans and mice. In addition, six consensus TCF/LEF-binding element (TBE) sites (site nos 8, 9, 10, 11, 12, and 13) and seven imperfect TBE sites (site nos 1, 2, 3, 4, 5, 6, and 7) are located in the upstream and genomic regions of human *ALEX1* gene, respectively (Fig. 1a). Luciferase reporter analysis showed that human *ALEX1* promoter (−1933 to +487), which included a CRE, an E-box, and eight TBE sites, was active in HCT116, SW480, and PANC-1 cells. The site-directed mutations of each CRE and E-box dramatically impaired the luciferase activities in HCT116, SW480, and PANC-1 cells, whereas the mutations of eight TBE sites slightly up-regulated the *ALEX1* promoter activity (Fig. 1b). In addition, co-transfection with a wild-type CREB expression vector induced approximately 4.3-, 2.0-, and 2.1-fold increase in

doi: 10.1111/j.1349-7006.2010.01541.x

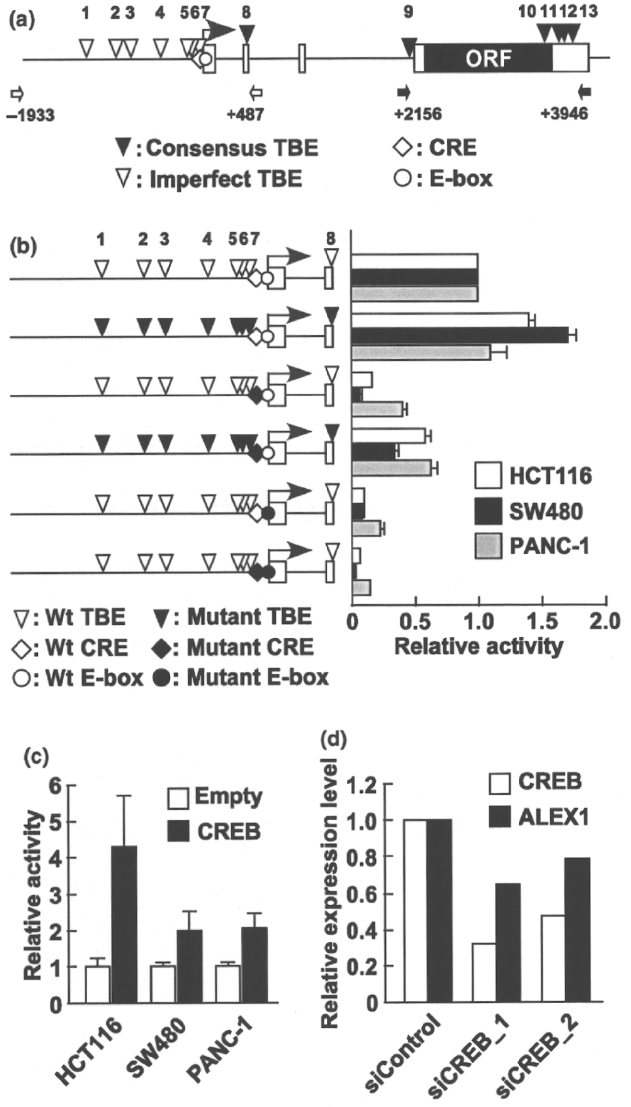

Fig. 1. The cyclic AMP response element (CRE) site and CRE-binding protein (CREB) are involved in human Arm protein lost in epithelial cancers, on chromosome X 1 (*ALEX1*) regulation. (a) A schematic representation of the genomic structure of the *ALEX1* gene on human chromosome X. Open and filled boxes represent the exons of the *ALEX1* gene and the ORF encoding the ALEX1 protein, respectively. The bent arrow indicates the transcription start site of the *ALEX1* gene. The positions of consensus (CTTTGA/TA/T and A/TA/TCAAAG) and imperfect TCF/LEF-binding element (TBE)s are indicated by filled and open reverse triangles, respectively, and numbered. An open diamond and circle represent the putative CRE (TGACGTG) and E-box (CACGTG) site, respectively. The open and closed arrows indicate the primers used for promoter and intron 3-exon 4 regions of the *ALEX1* gene, respectively. (b) In the left diagram, open reverse triangles represent wild-type TBE sites, and filled reverse triangles represent mutated TBE sites. Open and filled diamonds represent the wild-type and mutant type of CRE, respectively. Open and filled circles represent the wild-type and mutant type of E-box, respectively. The right bar graph represents the relative luciferase activities in HCT116, SW480, and PANC-1 cells transfected with the reporter plasmid driven by wild-type and a series of site-directed mutant type of the *ALEX1* promoter. Error bars indicate the SD. (c) Luciferase reporter assay of HCT116, SW480, and PANC-1 cells co-transfected with wild-type *ALEX1* promoter-driven reporter plasmid and the expression plasmid of the indicated genes. Error bars indicate the SD. (d) Quantitative real-time RT-PCR analysis of endogenous *CREB* and *ALEX1* mRNA expression in PANC-1 cells transfected with control siRNA and siRNAs targeting CREB. Relative expression level of *CREB* and *ALEX1* mRNA for each sample was normalized against the expression level of *GAPDH* mRNA. The average of two independent experiments is shown.

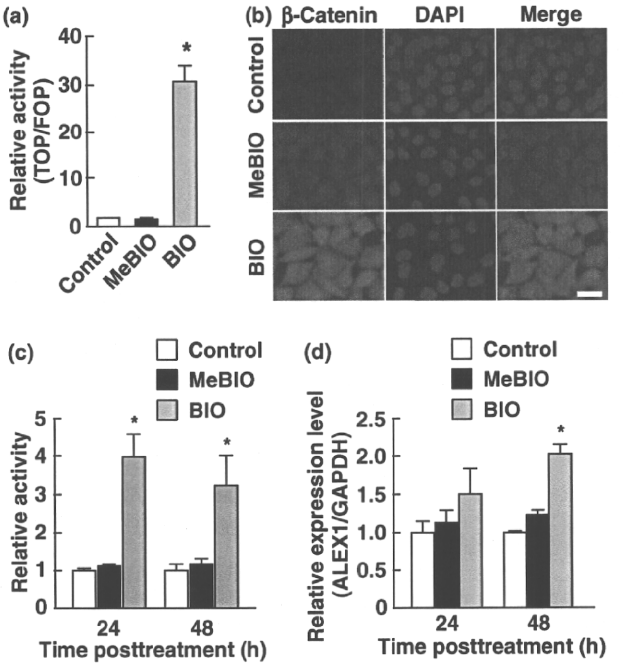

Fig. 2. Glycogen synthase kinase-3 (GSK-3) inhibitor induces human Arm protein lost in epithelial cancers, on chromosome X 1 (*ALEX1*) expression. Luciferase reporter assay of PANC-1 cells treated with/without a GSK-3 inhibitor, 6-bromoindirubin-3′-oxime (BIO), or an inactive analog of BIO, 1-mehyl-6-bromoindirubin-3′-oxime (MeBIO). The bar graph represents the mean ratios between the luciferase activities from TOPflash and FOPflash reporter (TOP/FOP ratio) (a), and relative activities driven by wild-type *ALEX1* promoter (c). (b) Indirect immunofluorescense analysis for β-catenin with PANC-1 cells treated with control solvent, MeBIO, and BIO. Nucleus was stained with DAPI. (d) Quantitative real-time RT-PCR analysis of endogenous *ALEX1* mRNA expressed in PANC-1 cells treated with BIO or MeBIO for 24 and 48 h. Relative expression level of *ALEX1* mRNA for each sample was normalized against the expression level of *GAPDH* mRNA. Error bars indicate the SD. $*P < 0.05$ compared to control and MeBIO-treated cells.

ALEX1 promoter activities in HCT116, SW480, and PANC-1 cells, respectively (Fig. 1c), whereas knockdown of *CREB* expression using two specific siRNAs decreased the *ALEX1* mRNA level in PANC-1 cells (Fig. 1d). These data indicate that both the CRE and E-box sites are essential *cis*-regulatory elements for basal promoter activity of the *ALEX1* gene, and CREB up-regulates the *ALEX1* promoter activity.

Continuous activation of β-catenin up-regulates *ALEX1* expression. The consensus TBE sequence recognized by the β-catenin/TCF complex locates in the proximal promoter regions of several known target genes of canonical Wnt signaling[6,7,14]. To determine whether *ALEX1* gene expression is regulated by Wnt/β-catenin signaling, we examined the expression level and promoter activity of the *ALEX1* gene in GSK-3 inhibitor-treated PANC-1 cells. PANC-1 cells exhibited low levels of β-catenin expression and β-catenin/TCF transcriptional activity (Figs 2a, 3a), and detectable level of endogenous *ALEX1* mRNA by RT-PCR. Activation of the β-catenin/TCF target promoter (TOPflash) and cytoplasmic and nuclear accumulation of β-catenin were markedly induced by GSK-3 inhibitor BIO, but not by MeBIO (a kinase-inactive analog of BIO) (Fig. 2a,b). The luciferase activity of *ALEX1* promoter-driven reporter plasmid was also increased in BIO-treated PANC-1 cells 24 h and 48 h post treatment in comparison to that in solvent-treated control and MeBIO-treated PANC-1 cells (Fig. 2c). In addition, quantitative real-time RT-PCR revealed an increase of endogenous *ALEX1*

mRNA by BIO-treatment (Fig. 2d). Lithium chloride, which is known to function as a GSK-3 inhibitor, also induced an increase of *ALEX1* mRNA (data not shown). These results demonstrate that activation of Wnt/β-catenin signaling by GSK-3 inhibition up-regulates the promoter activity and gene expression of *ALEX1*.

Furthermore, to validate whether cytoplasmic and nuclear accumulation of β-catenin using genetic mutant also activates the *ALEX1* gene, we generated the stable clones of PANC-1 cells expressing the degradation-resistant β-catenin mutant with a deletion of Ser^{45}, which is a phosphorylation site for GSK-3β priming, designated as PANC-1/β-catenin-ΔS45. As a result, two PANC-1/β-catenin-ΔS45 clones showed higher expression levels of β-catenin protein and activation of the target promoter of β-catenin/TCF compared with those in the control PANC-1/empty and PANC-1/EGFP clones (Fig. 3a,b). Quantitative real-time RT-PCR and luciferase reporter analysis revealed significant elevations of endogenous mRNA expression and promoter activity of *ALEX1* in the PANC-1/β-catenin-ΔS45 clones (Fig. 3c,d), indicating that *ALEX1* gene is regulated by Wnt/β-catenin signaling.

Regulation of *ALEX1* gene expression by β-catenin is CRE dependent. Since comparable induction by BIO was obtained using the *ALEX1* promoter-driven reporter plasmids with/without intron 3-exon 4 region containing five TBE sites (+2156 to +3946; Fig. 4a), we used the *ALEX1* promoter-driven reporter plasmid without intron 3-exon 4 region to elucidate a regulatory region required for β-catenin stimulation. A series of 5′ deletions and site-directed mutations of TBE sites exhibited little impairment in response to Wnt/β-catenin signaling induced by BIO (Fig. 4b). Furthermore, the activation of the *ALEX1* promoter was suppressed by the overexpression of the N-terminal deletion mutant of TCF4 (ΔN-TCF4) known to block the transcriptional activity of β-catenin due to lack of the β-catenin binding domain (Fig. 4c). Previous studies have reported that transcription factors, including CREB, are capable of recruiting β-catenin;[10,15–17] thus, we evaluated the effect of the CRE site on β-catenin-mediated transactivation of the *ALEX1* promoter by luciferase reporter assay. Interestingly, the mutation of the CRE site resulted in almost complete loss of induction by BIO (Fig. 4b). These data suggest that the CRE site plays an important role in mediating β-catenin-dependent transcriptional activation of the *ALEX1* promoter, whereas the TBE sites play only a minor role although TCF4 may contribute to this activation.

The transcriptional relevance of CREB in regulating the *ALEX1* expression in the PANC-1/empty and the PANC-1/β-catenin-ΔS45 clones was further confirmed by ChIP assay (Fig. 4d). To further investigate whether CREB mediates activation of the *ALEX1* promoter by β-catenin, wild-type CREB and two dominant-negative mutants, $CREB^{R287L}$ and $CREB^{S119A}$, were overexpressed in BIO-treated PANC-1 cells. The luciferase reporter analysis for the *ALEX1* promoter showed that the response to β-catenin was enhanced by the wild-type CREB but was suppressed by a DNA-binding defective mutant $CREB^{R287L}$ (Fig. 4c), indicating that CREB, at least in part, mediates the transcriptional activation of the *ALEX1* gene by Wnt/β-catenin signaling. Surprisingly, a Ser^{119} phosphorylation-defective mutant $CREB^{S119A}$ enhanced the activation of the *ALEX1* promoter by BIO, suggesting that BIO-induced activation of the *ALEX1* promoter is independent of the phosphorylation of CREB at Ser^{119} which is important for transcriptional activation of several CREB target genes.

Discussion

Arm family members exert diverse functions through interactions of their Arm repeat domain with several binding partners.

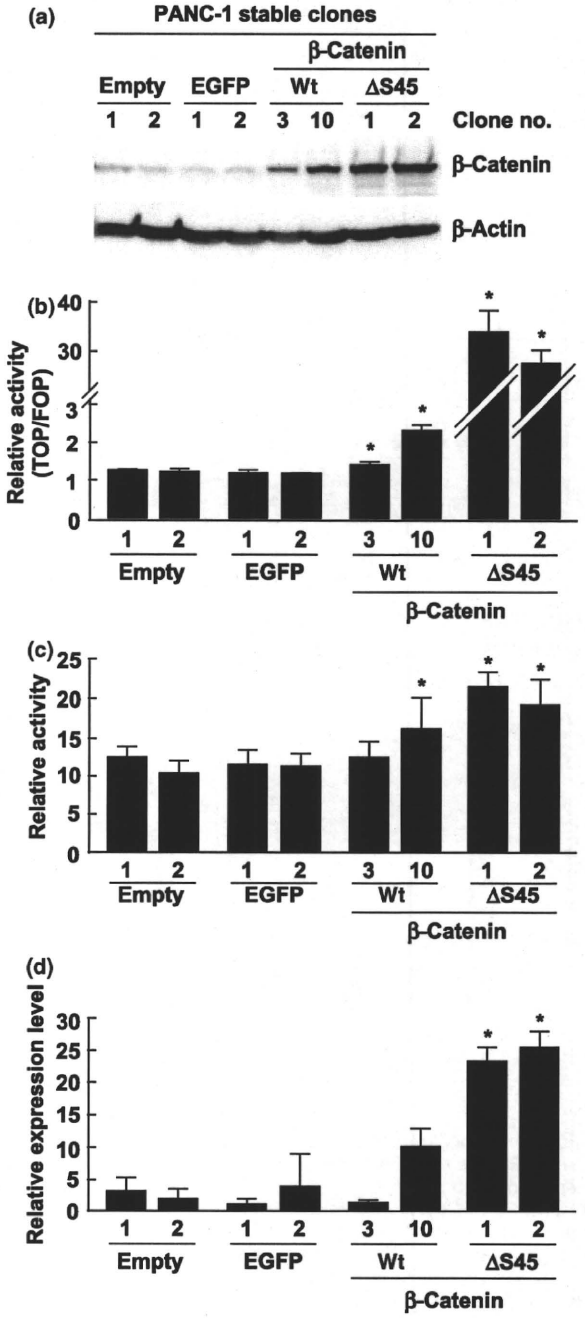

Fig. 3. Overexpression of the constitutive-active mutant type of β-catenin induces human Arm protein lost in epithelial cancers, on chromosome X 1 (*ALEX1*) expression. (a) Western blot analysis for β-catenin was performed with the cell lysate from stably transfected PANC-1/empty, PANC-1/EGFP, PANC-1/β-catenin-wt, and PANC-1/β-catenin-ΔS45 clones. β-Actin protein served as an internal control. (b) Luciferase reporter assay of stably transfected PANC-1 clones transfected with reporter constructs. The bar graph represents the mean ratios between the luciferase activities from TOPflash and FOPflash reporter (TOP/FOP ratio). The error bars represent the SD. $*P < 0.05$ compared to each control clone (empty nos 1 and 2, and EGFP nos 1 and 2). (c) Luciferase reporter assay of each stably transfected PANC-1 clone transfected with wild-type *ALEX1* promoter-driven reporter plasmid. The bar graph represents the relative luciferase activities, and the error bars represent the SD. $*P < 0.05$ compared to each control clone (empty nos 1 and 2, and EGFP nos 1 and 2). (d) Quantitative real-time RT-PCR analysis of endogenous *ALEX1* mRNA of stably transfected PANC-1 clone. The relative level of *ALEX1* mRNA expression for each sample was normalized against the expression level of *GAPDH* mRNA. $*P < 0.05$ compared to each control clone (empty nos 1 and 2, and EGFP nos 1 and 2).

doi: 10.1111/j.1349-7006.2010.01541.x

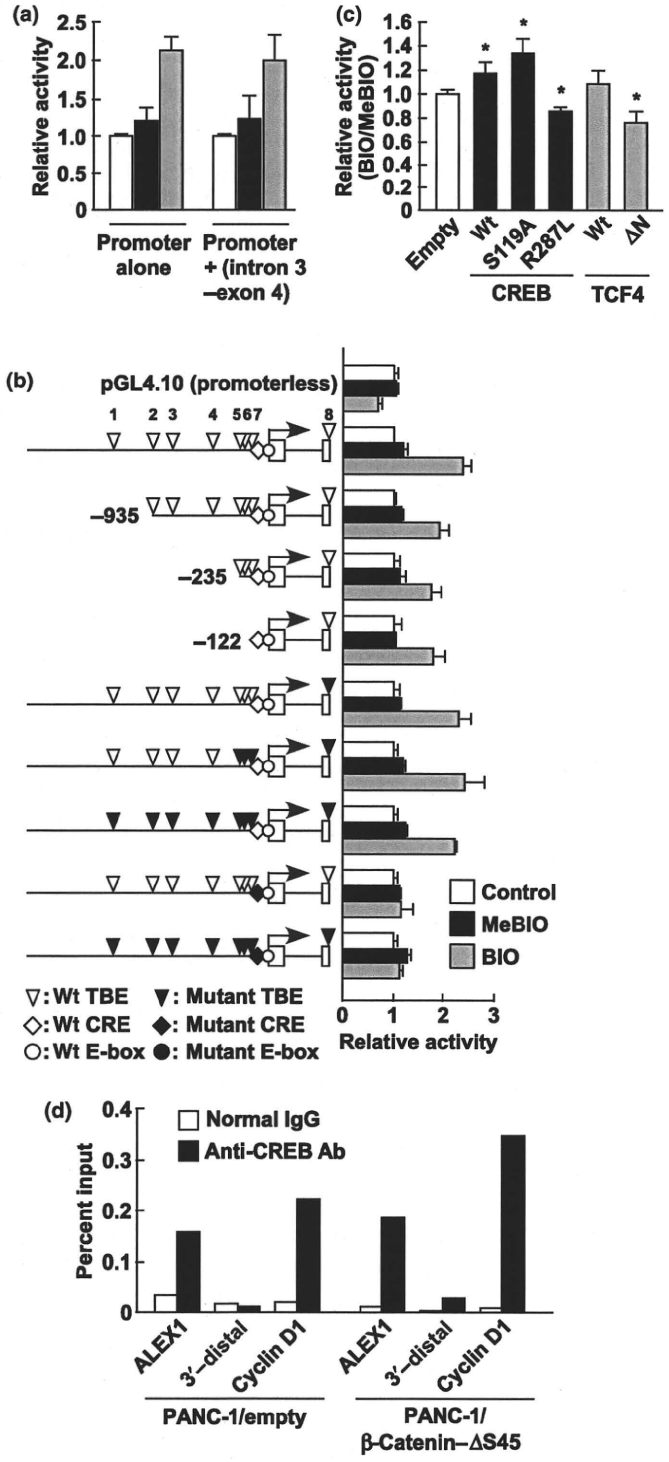

Fig. 4. Cyclic AMP response element (CRE)-site and CRE-binding protein (CREB)-mediated activation of human Arm protein lost in epithelial cancers, on chromosome X1 (*ALEX1*) promoter by the glycogen synthase kinase-3 (GSK-3) inhibitor. (a) Luciferase reporter assay of PANC-1 cells transfected with wild-type *ALEX1* promoter-driven reporter plasmid with/without the intron 3-exon 4 region containing five TBE sites (+2156 to +3946). The bar graph represents the relative luciferase activities. (b) The left diagram is shown as described in the legend for Figure 1(b). The right bar graph represents the relative luciferase activities in control, 1-mehyl-6-bromoindirubin-3′-oxime (MeBIO)-, and 6-bromoindirubin-3′-oxime (BIO)-treated PANC-1 cells transfected with the reporter plasmid driven by wild-type, a series of 5′ deleted type, or a series of the site-directed mutant type of human *ALEX1* promoter. The error bars indicate the SD. (c) Luciferase reporter assay of PANC-1 cells co-transfected with wild-type *ALEX1* promoter-driven reporter plasmid and expression plasmid of the indicated genes. The bar graph represents the mean ratios between the luciferase activities in PANC-1 cells treated with BIO and MeBIO (BIO/MeBIO ratio), and the error bars represent the SD. $*P < 0.05$ compared to control (empty). (d) Chromatin immunoprecipitation followed by quantitative real-time PCR was carried out with normal rabbit IgG or anti-CREB antibody using the PANC-1/empty clone 1 and PANC-1/β-catenin-ΔS45 clone 1. Sequences of cyclin D1 promoter and 3′-distal region of the *ALEX1* gene were used as a positive and negative control for CREB binding, respectively.

ALEX1 and its homologs are not classical members of the Arm family and represent a new family of proteins with less than six Arm repeats. Here we revealed the *cis*-regulatory elements and *trans*-acting factors involved in the transcriptional regulation of the *ALEX1* gene. First, we demonstrated that potential CRE and E-box sites were essential *cis*-regulatory elements for basal transcription of the human *ALEX1* gene. A CRE and an E-box are known to be occupied by the CREB/ATF family and the basic helix-loop-helix family of transcription factors, respectively. Since overexpression and knockdown of CREB altered the *ALEX1* promoter activity, CREB may play an important role in regulating *ALEX1* gene expression. In addition, ChIP assay also supported the role of CREB in transcriptional activation of the *ALEX1* gene via binding to the proximal promoter region including the CRE site. However, the response of the *ALEX1* promoter to CREB induction was not diminished by the CRE mutation (Fig. S1, Supporting information). Several genes have been found to be regulated by CREB via multiple CRE sites, and point mutations in one CRE site alone are not enough to impair its promoter activity. Luciferase reporter analysis using a series of 5′ deletions of the *ALEX1* promoter-driven vector suggests that at least the proximal promoter region (−122 to +487) contains a CREB response sequence (Fig. S1, Supporting information). In the case of the *ALEX1* gene, CREB might regulate via multiple CRE sites which are uncovered in this paper. Further studies are needed to identify transcription factors regulating *ALEX1* gene expression through the E-box site. Second, we showed that Wnt/β-catenin signaling up-regulated *ALEX1* gene expression and transcriptional activation of the *ALEX1* gene by β-catenin mediated by the CRE site. It is believed that β-catenin binds DNA indirectly through the interaction with a member of the TCF/LEF family because β-catenin does not possess a DNA-binding domain.[18] However, a genome-wide analysis of β-catenin occupancy revealed a lack of consensus TBE motif in 16% of target genes,[19] suggesting that β-catenin binds to this group of targets indirectly through a nonconsensus TBE motif or an unrelated factor-binding site. In fact, the transcription factors FOXO, Pit1, and Prop1 recruit β-catenin to their target gene promoters.[15–17] Furthermore, recent studies have provided evidence supporting the importance of CRE sites in Wnt signaling, since interaction with CREB is required for β-catenin to activate the cyclin D1 and cyclooxygenase-2 promoter.[10,20] In this report, a GSK-3 inhibitor and β-catenin up-regulated *ALEX1* gene expression (Figs 2,3). Importantly, BIO-induced activation of the *ALEX1* promoter was little affected by the mutations of TBE sites, but almost completely abolished by the mutation of the CRE site (Fig. 4a). Moreover, overexpression of CREB enhanced BIO-induced *ALEX1* promoter activation (Fig. 4b). Taken together, *ALEX1* is thought to be regulated by Wnt/β-catenin signaling; however, the regulation of *ALEX1* gene expression by β-catenin may be mediated by the CRE but not TBE sites. Third, the CREB-mediated regulation of *ALEX1* gene expression by β-catenin was CREB phosphorylation independent. The $CREB^{R287L}$ mutant, which blocks binding of wild-type CREB to CRE sites through heterodimer formation,[21] was

observed to reduce the response to β-catenin (Fig. 4c). However, the overexpression of the $CREB^{S119A}$ mutant, which underwent a point mutation at a potential phosphorylation site by several kinases such as a cAMP-dependent protein kinase, was observed to accelerate responses to β-catenin at similar levels of induction as those by overexpression of wild-type CREB (Fig. 4c). The phosphorylation of Ser^{119} is essential for the transcriptional activation of CREB, but not for DNA binding.[8] Therefore, the binding of CREB to the CRE sites is considered to be a prerequisite for the transcriptional activation of the *ALEX1* gene by β-catenin, and CREB phosphorylation may be dispensable for this activation.

The dysregulation of the Wnt signaling can contribute to tumor development mainly by activation of target gene expression such as c-*myc* and cyclin D1, whereas Wnt antagonists such as secreted frizzled-related proteins, dickkopf-1, and Wnt inhibitor factor-1 are also up-regulated by Wnt signaling, leading to the negative feedback regulation of Wnt signaling. The present data indicate that *ALEX1* is regulated by Wnt/β-catenin signaling. In addition, overexpression of ALEX1 suppresses the colony formation of colorectal cancer cell lines and is frequently down-regulated in human colorectal cancer (manuscript in preparation). Thus, it is speculated that ALEX1 might act as a negative regulator of cell proliferation promoted by aberrant activation of Wnt/β-catenin signaling.

In summary, the current results indicate that *ALEX1* is a potential target gene of CREB, and Wnt/β-catenin signaling regulates *ALEX1* gene expression. The CRE is important for basal promoter activity and the transcriptional activation of *ALEX1* gene response to β-catenin. This is the first study to investigate the transcriptional regulation of the ALEX family, and these findings may provide new insights into the molecular mechanism underlying the CREB function and Wnt/β-catenin signaling.

Acknowledgments

The authors thank Hitoshi Niwa of the RIKEN Center for Developmental Biology for the generous gift of the pCAGIPuro and pCAGIPuro/EGFP plasmids. The authors also thank members of the Division of Functional Genomics and Systems Medicine for helpful discussion and advice. This work was partly supported by a Grant-in-Aid for Development of New Technology from The Promotion and Mutual Aid Corporation for Private Schools of Japan (2008).

References

1 Reya T, Clevers H. Wnt signalling in stem cells and cancer. *Nature* 2005; **434**: 843–50.
2 Katoh M. WNT signaling pathway and stem cell signaling network. *Clin Cancer Res* 2007; **13**: 4042–5.
3 Goss KH, Groden J. Biology of the adenomatous polyposis coli tumor suppressor. *J Clin Oncol* 2000; **18**: 1967–79.
4 Wong SC, Lo ES, Lee KC, Chan JK, Hsiao WL. Prognostic and diagnostic significance of β-catenin nuclear immunostaining in colorectal cancer. *Clin Cancer Res* 2004; **10**: 1401–8.
5 Shtutman M, Zhurinsky J, Simcha I *et al.* The cyclin D1 gene is a target of the b-catenin/LEF-1 pathway. *Proc Natl Acad Sci USA* 1999; **96**: 5522–7.
6 He TC, Sparks AB, Rago C *et al.* Identification of c-MYC as a target of the APC pathway. *Science* 1998; **281**: 1509–12.
7 Tetsu O, McCormick F. β-Catenin regulates expression of cyclin D1 in colon carcinoma cells. *Nature* 1999; **398**: 422–6.
8 Mayr B, Montminy M. Transcriptional regulation by the phosphorylation-dependent factor CREB. *Nat Rev Mol Cell Biol* 2001; **2**: 599–609.
9 Xu L, Corcoran RB, Welsh JW, Pennica D, Levine AJ. WISP-1 is a Wnt-1- and b-catenin-responsive oncogene. *Genes Dev* 2000; **14**: 585–95.
10 Pradeep A, Sharma C, Sathyanarayana P *et al.* Gastrin-mediated activation of cyclin D1 transcription involves β-catenin and CREB pathways in gastric cancer cells. *Oncogene* 2004; **23**: 3689–99.
11 Giese K, Kingsley C, Kirshner JR, Grosschedl R. Assembly and function of a TCRα enhancer complex is dependent on LEF-1-induced DNA bending and multiple protein-protein interactions. *Genes Dev* 1995; **9**: 995–1008.
12 Kurochkin IV, Yonemitsu N, Funahashi SI, Nomura H. ALEX1, a novel human armadillo repeat protein that is expressed differentially in normal tissues and carcinomas. *Biochem Biophys Res Commun* 2001; **280**: 340–7.
13 Smith CA, McClive PJ, Sinclair AH. Temporal and spatial expression profile of the novel armadillo-related gene, Alex2, during testicular differentiation in the mouse embryo. *Dev Dyn* 2005; **233**: 188–93.
14 Easwaran V, Lee SH, Inge L *et al.* β-Catenin regulates vascular endothelial growth factor expression in colon cancer. *Cancer Res* 2003; **63**: 3145–53.
15 Kioussi C, Briata P, Baek SH *et al.* Identification of a Wnt/Dvl/β-Catenin –> Pitx2 pathway mediating cell-type-specific proliferation during development. *Cell* 2002; **111**: 673–85.
16 Olson LE, Tollkuhn J, Scafoglio C *et al.* Homeodomain-mediated β-catenin-dependent switching events dictate cell-lineage determination. *Cell* 2006; **125**: 593–605.
17 Essers MA, de Vries-Smits LM, Barker N, Polderman PE, Burgering BM, Korswagen HC. Functional interaction between β-catenin and FOXO in oxidative stress signaling. *Science* 2005; **308**: 1181–4.
18 Xu W, Kimelman D. Mechanistic insights from structural studies of β-catenin and its binding partners. *J Cell Sci* 2007; **120**: 3337–44.
19 Yochum GS, McWeeney S, Rajaraman V, Cleland R, Peters S, Goodman RH. Serial analysis of chromatin occupancy identifies β-catenin target genes in colorectal carcinoma cells. *Proc Natl Acad Sci USA* 2007; **104**: 3324–9.
20 Wang H, Wen S, Bunnett NW, Leduc R, Hollenberg MD, MacNaughton WK. Proteinase-activated receptor-2 induces cyclooxygenase-2 expression through β-catenin and cyclic AMP-response element-binding protein. *J Biol Chem* 2008; **283**: 809–15.
21 Shaywitz AJ, Greenberg ME. CREB: a stimulus-induced transcription factor activated by a diverse array of extracellular signals. *Annu Rev Biochem* 1999; **68**: 821–61.

Supporting Information

Additional Supporting Information may be found in the online version of this article:

Table S1. Primer sequences used in this study.

Fig. S1. The proximal regulatory region of the Arm protein lost in epithelial cancers, on chromosome X 1 (*ALEX1*) gene responds to cyclic AMP response element binding protein (CREB) induction. Luciferase reporter assay of PANC-1 cells co-transfected with the reporter plasmid driven by a series of deletion and site-directed mutant types of the ALEX1 promoter, and the CREB expression plasmid or control empty plasmid. Error bars indicate the SD.

Please note: Wiley-Blackwell are not responsible for the content or functionality of any supporting materials supplied by the authors. Any queries (other than missing material) should be directed to the corresponding author for the article.

doi: 10.1111/j.1349-7006.2010.01541.x

THE JOURNAL OF BIOLOGICAL CHEMISTRY VOL. 285, NO. 20, pp. 15577–15586, May 14, 2010

Dual Roles of Smad Proteins in the Conversion from Myoblasts to Osteoblastic Cells by Bone Morphogenetic Proteins*[S]

Received for publication, May 31, 2009, and in revised form, March 5, 2010 Published, JBC Papers in Press, March 15, 2010, DOI 10.1074/jbc.M109.028019

Junya Nojima[‡§], Kazuhiro Kanomata[‡], Yumi Takada[¶], Toru Fukuda[‡], Shoichiro Kokabu[‡§], Satoshi Ohte[‡], Takatora Takada[¶], Tohru Tsukui[‖], Takamasa S. Yamamoto[**], Hiroki Sasanuma[‡], Katsumi Yoneyama[‡], Naoto Ueno[**], Yasushi Okazaki[‡‡], Ryutaro Kamijo[¶], Tetsuya Yoda[§], and Takenobu Katagiri[‡1]

From the Divisions of [‡]Pathophysiology, [‖]Experimental Animal Laboratory, and [‡‡]Functional Genomics and System Research, Research Center for Genomic Medicine, Saitama Medical University, 1397-1 Yamane, Hidaka-shi, Saitama 350-1241, the [§]Department of Oral and Maxillofacial Surgery, Faculty of Medicine, Saitama Medical University, 38 Moro Hongo, Moroyama-machi, Iruma-gun, Saitama 350-0495, the [¶]Department of Biochemistry, School of Dentistry, Showa University, 1-5-8 Hatanodai, Shinagawa-ku, Tokyo 142-5555, and the [**]Division of Morphogenesis, Department of Developmental Biology, National Institute for Basic Biology, 38 Nishigonaka, Myodaiji, Okazaki, Aichi 444-8585, Japan

Bone morphogenetic proteins (BMPs) induce ectopic bone formation in muscle tissue *in vivo* and convert myoblasts such that they differentiate into osteoblastic cells *in vitro*. We report here that constitutively active Smad1 induced osteoblastic differentiation of C2C12 myoblasts in cooperation with Smad4 or Runx2. In floxed Smad4 mice-derived cells, Smad4 ablation partially suppressed BMP-4-induced osteoblast differentiation. In contrast, the BMP-4-induced inhibition of myogenesis was lost by Smad4 ablation and restored by Smad4 overexpression. A nuclear zinc finger protein, E4F1, was identified as a possible component of the Smad4 complex that suppresses myogenic differentiation in response to BMP signaling. In the presence of Smad4, E4F1 stimulated the expression of *Ids*. Taken together, these findings suggest that the Smad signaling pathway may play a dual role in the BMP-induced conversion of myoblasts to osteoblastic cells.

Bone morphogenetic proteins (BMPs)[2] are members of the transforming growth factor-β (TGF-β) superfamily, which regulates the differentiation, proliferation, and death of various types of cells (1). BMPs were originally found in bone matrix as factors responsible for the induction of ectopic bone formation, in which implantation of demineralized bone matrix into muscle tissue induced new bone tissue containing bone marrow (2, 3). Implantation of individual recombinant BMPs, such as BMP-2, BMP-4, BMP-6, and BMP-7, into muscle tissue induces ectopic bone formation *in vivo* as well (4). This ectopic bone-inducing activity is highly specific to BMPs, because other hormones and cytokines, including TGF-β1 itself, failed to induce ectopic bone formation in muscle tissue *in vivo* (5). Although many factors, such as BMPs, TGF-βs, fibroblast growth factors, and epidermal growth factor, inhibit myogenic maturation of myoblasts *in vitro*, only BMPs convert them so that they differentiate to osteoblastic cells, the bone-forming cells in vertebrates (6–10). Thus, the activity of BMPs in myoblast cultures to induce osteoblastic differentiation appears to reflect the ectopic bone-inducing activity of BMPs *in vivo* (8).

BMP signaling is transduced by two different types of serine/threonine kinase receptors, termed type I and II receptors (1, 11, 12). The BMP-bound type II receptor phosphorylates the type I receptor kinase, and the activated BMP type I receptor in turn phosphorylates downstream substrates such as receptor-regulated Smads (R-Smads), including Smad1, Smad5, and Smad8 and p38 mitogen-activated protein kinase. Phosphorylated R-Smads form heteromeric complexes with Smad4 and translocate into the nucleus to regulate transcription of various target genes, including *Id1*, which encodes a dominant-negative inhibitor of myogenesis (13–15). Recently, a genetic mutation of ALK2, a BMP type I receptor, was identified in patients with fibrodysplasia ossificans progressiva, an autosomal-dominant disorder characterized by heterotopic bone formation in muscle tissue (16). Our findings indicate that this mutant ALK2 is a constitutively activated and hyper-reactive form of the BMP type I receptor and suggest that downstream signaling of activated receptors play an important role in heterotopic bone formation in muscle tissue under certain pathological conditions (17).

Here, we show that a protein in which the carboxyl-terminal serine residues of Smad1 were substituted with aspartic acids, termed Smad1(DVD), functioned as a constitutively activated

* This work was supported in part by Health and Labor Sciences Research Grants for Research on Measures for Intractable Research from the Ministry of Health, Labor and Welfare of Japan (to T. K.), grant-in-aids from Saitama Medical University Internal Grants (to T. F. and T. K.), grant-in-aids from the Ministry of Education, Culture, Sports, Science, and Technology of Japan (to T. F. and T. K.), a grant-in-aid for "Support Project of Strategic Research Center in Private Universities" from the Ministry of Education, Culture, Sports, Science and Technology of Japan to Saitama Medical University Research Center for Genomic Medicine (to T. K.), a grant-in-aid from the Sankyo Foundation of Life Science (to T. K.), a grant-in-aid from the Kawano Masanori Memorial Foundation for Promotion of Pediatrics (to T. K.), a grant-in-aid from the Novo Nordisk Award for Growth and Development (to T. K.), a grant-in-aid from Japan Intractable Diseases Research Foundation (to T. F.), and a grant-in-aid from the Takeda Science Foundation (to T. K.).

[S] The on-line version of this article (available at http://www.jbc.org) contains supplemental Figs. S1–S3.

[1] To whom correspondence should be addressed. Tel.: 81-42-984-0443; Fax: 81-42-984-4651; E-mail: katagiri@saitama-med.ac.jp.

[2] The abbreviations used are: BMP, bone morphogenetic protein; ALP, alkaline phosphatase; BMPR-IA, bone morphogenetic protein receptor type IA; MHC, myosin heavy chain; TGF-β, transforming growth factor-β; ChIP, chromatin immunoprecipitation; NLS, nuclear localization signal; EGFP, enhanced green fluorescent protein; MEF, mouse embryonic fibroblast; RNAi, RNA interference; siRNA, small interfering RNA; R-Smad, receptor-regulated Smad; luc, luciferase.

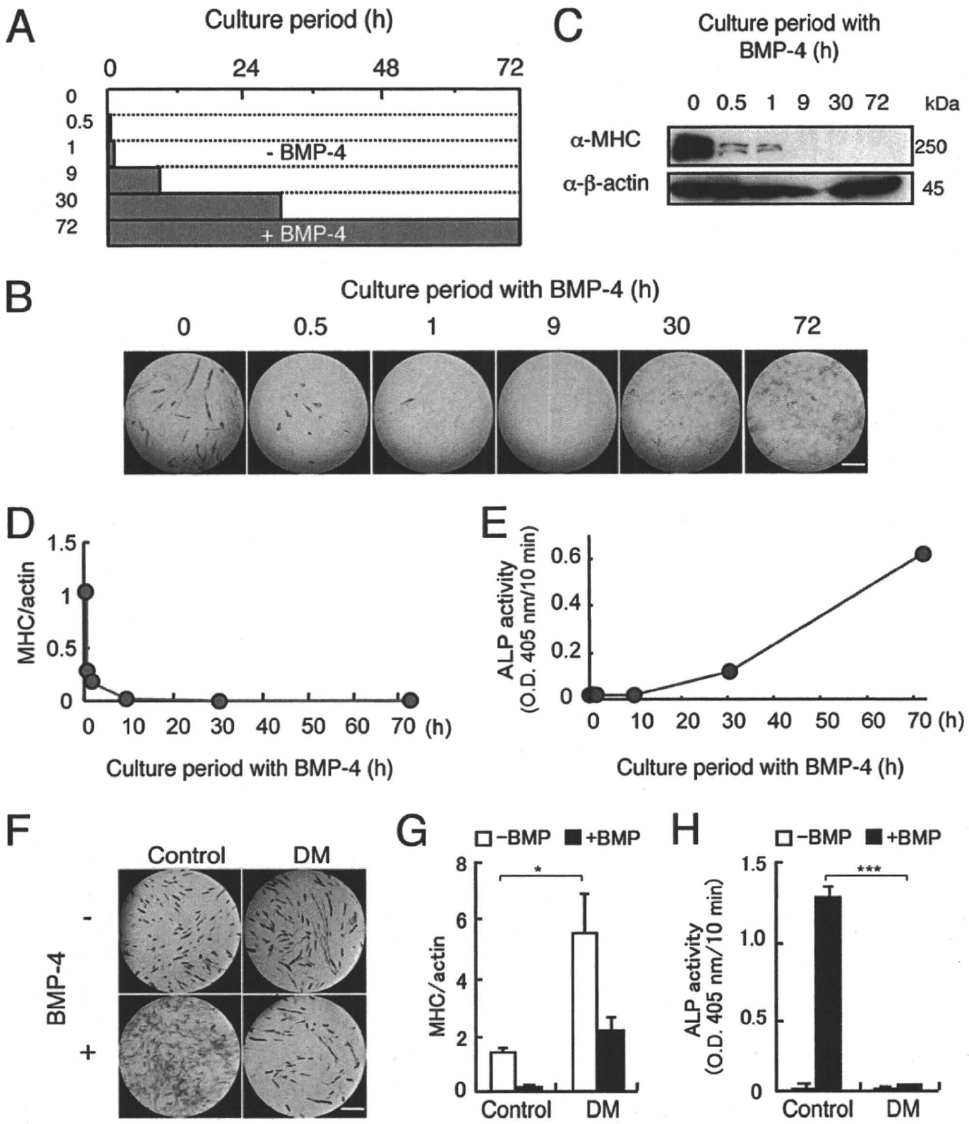

FIGURE 1. **Smad signaling pathway regulates both inhibition of myogenic differentiation and induction of osteoblastic differentiation by BMP-4.** *A* and *B*, examination of the minimal treatment periods required for inhibition of myogenic differentiation and induction of osteoblastic differentiation by BMP-4 in C2C12 myoblasts. *A*, scheme of treatment of C2C12 myoblasts with BMP-4 in a window experiment. C2C12 cells were treated for 0, 0.5, 1, 9, 30, or 72 h with 100 ng/ml of BMP-4 (*closed bars*) and further incubated without BMP-4 (*open bars*) until 72 h before staining. *B*, the cells were doubly stained for ALP and MHC in *blue* and *red*, respectively, at 72 h. *Scale bar*, 200 μm. *C–E*, quantitation of the effects of BMP-4 on myogenic differentiation and osteoblastic differentiation of C2C12 cells. Western blots for MHC (*C* and *D*) and measurement of ALP activity (*E*) were performed on day 3. *F–H*, effects of Dorsomorphin on BMP-induced differentiation in C2C12 cells. C2C12 cells were preincubated for 1 h with 3 μM Dorsomorphin (DM) and 100 ng/ml of BMP-4 was then added. *F*, the cells were doubly stained for ALP and MHC on day 3. *Scale bar*, 400 μm. MHC levels (*G*) and ALP activity (*H*) were measured on day 3. Values are mean ± S.D. ($n = 3$). *, $p < 0.05$; ***, $p < 0.001$.

Smad1. Overexpression of Smad1(DVD) induced osteoblastic differentiation of C2C12 myoblasts, although the inhibition of myogenic differentiation depended principally on nuclear Smad4 rather than R-Smads. E4F1 was identified as a possible component of the Smad4 complex in the suppression of myogenic differentiation by BMP signaling. R-Smads and Smad4 play important roles in the conversion of myogenic cells to osteoblastic cells by BMPs, data were confirmed with the deletion of Smad4 in mouse embryonic fibroblasts (MEFs).

EXPERIMENTAL PROCEDURES

Expression Vectors—Expression vectors for wild-type mouse Smad1, Smad4, and Smad7 were described previously (13). All of the mutations were introduced by a standard PCR technique using Platinum Pfx DNA polymerase (Invitrogen) and their sequences were confirmed in each expression vector. Smad1 mutants were obtained by substitution of Ser-463 and/or Ser-465 of mouse Smad1 with aspartic acid or alanine residues. A nuclear localization signal derived from an SV40 large T antigen, PPKKKRKV, was inserted between an amino-terminal epitope tag and Smad1 or Smad4. NLS-Smad4(ΔMH1) and NLS-Smad4(ΔMH2) were obtained by deleting amino acids 2–138 and 316–552, respectively, from full-length NLS-Smad4. Both mouse wild-type and dominant-negative Runx2 vectors were kindly provided by Dr. Toshihisa Komori (Nagasaki University) (18). Mouse *E4f1* (accession number BC057011) cDNA was obtained by a standard reverse transcription-PCR technique and cloned into pcDEF3 with a FLAG epitope sequence at the 3′ end (19), and E4F1(ΔE3) and the zinc finger mutants (Z1–Z6) were generated by deleting a ubiquitin E3 ligase domain, amino acids 40–84, and substituting two cysteine residues with alanines at positions 195 and 197, 223 and 226, 435 and 438, 519 and 522, and 547 and 550, respectively.

Cell Cultures and Transfections—C2C12 mouse myoblasts, C3H10T1/2 mouse fibroblasts, and COS-7 African green monkey kidney cells were maintained as described (8, 20). The cells were treated with 100 ng/ml of recombinant human BMP-4 (R & D Systems, Inc.) in the presence or absence of chemical inhibitors of mitogen-activated protein kinase, U0126, SB203580, or SP600125 (Merck, Tokyo, Japan) or of the BMP Smad pathway, Dorsomorphin (Calbiochem, San Diego, CA) (20, 21). Lipofectamine 2000 (Invitrogen) was used for plasmid transfections. RNAi Stealth oligonucleotides against murine *Smad1* (MSS275578), *Smad5* (MSS2755978), *Runx2* (MSS202675), *Smad4* (MSS206437), and *E4f1* (MSS274050) and a scrambled negative control oligonucleotide were purchased from Invitrogen. An expression plasmid for *E4f1* microRNA was constructed by subcloning Mmi508063 (Invitrogen) into pcDNA6.2-GW/EmGFP-miR (Invitrogen). MEFs prepared from *Smad4*$^{floxed/floxed}$ mouse embryos at 11.5 days postcoitum were infected with an

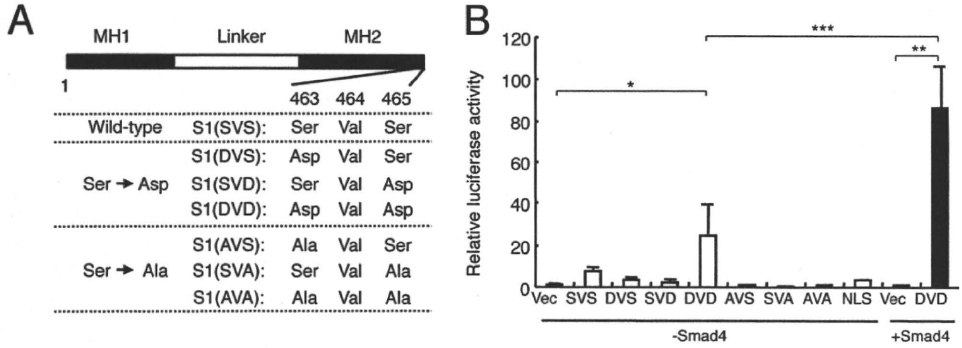

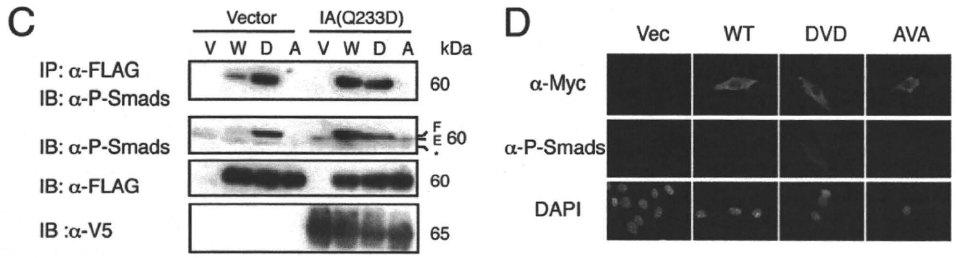

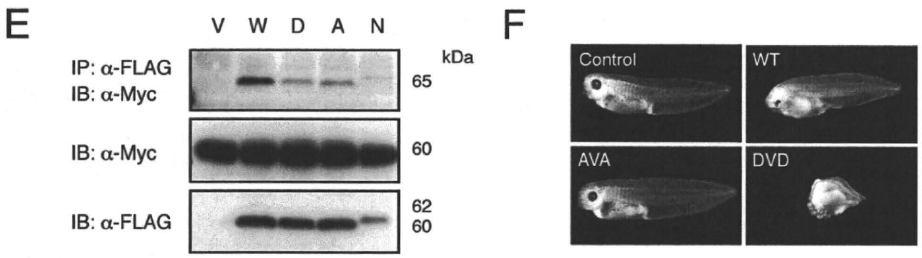

G

	Viability	DAI (dorso-anterior index)					Average	Others
		5	4	3	2	1		
Control	34 (100)	33 (97.1)	0 (0.0)	0 (0.0)	0 (0.0)	0 (0.0)	5.00	1 (2.9)
Smad1 WT	34 (100)	1 (2.9)	22 (64.7)	7 (20.6)	3 (8.8)	0 (0.0)	3.64	1 (2.9)
Smad1(AVA)	34 (100)	29 (85.3)	0 (0.0)	0 (0.0)	0 (0.0)	0 (0.0)	5.00	5 (14.7)
Smad1(DVD)	34 (100)	0 (0.0)	0 (0.0)	9 (26.5)	9 (26.5)	16 (47.1)	1.79	0 (0.0)

FIGURE 2. **Establishment of a constitutively activated Smad1.** *A*, construction of mutant Smad1. Serine 463 and/or 465 at the carboxyl terminus of mouse Smad1 was substituted by aspartic acid or alanine. *B*, transcriptional activities of Smad1 mutants in luciferase assay in C2C12 cells. Wild-type and mutant *Smad1* were transfected with IdWT4F-luc in C2C12 cells in the presence or absence of *Smad4* ($n = 3$). Note that Smad1(DVD) activated the reporter activity even in the absence of *Smad4*. *, $p < 0.05$; **, $p < 0.01$; ***, $p < 0.001$. *C* and *D*, Smad1(DVD) was recognized by the α-phospho-Smad1/5/8 antibody. C2C12 cells were co-transfected with empty vector (*Vector*) or V5-tagged *Bmpr-Ia*(*Q233D*) (*IA*(*Q233D*)) and an empty vector (*V*), FLAG-tagged wild-type *Smad1* (*W*), *Smad1*(*DVD*) (*D*), or *Smad1*(*AVA*) (*A*). Whole cell lysates were immunoprecipitated (*IP*) with anti-FLAG antibody followed by immunoblotting (*IB*) using α-P-Smads antibody to detect the mutant Smad1 and endogenous Smad1/5/8. *D*, C2C12 cells transfected with Myc-tagged wild-type or *Smad1*(*DVD*), *Smad1*(*AVA*), or *NLS-Smad1* were stained with α-P-Smads and α-Myc antibodies without BMP stimulation. Note that Smad1(DVD) was detected in the cytoplasm with α-P-Smads antibody. *E*, interaction with Smad1 and Smad4. C2C12 cells were co-transfected with Myc-tagged *Smad4* and an empty vector (*V*), FLAG-tagged wild-type *Smad1* (*W*), *Smad1*(*DVD*) (*D*), *Smad1*(*AVA*) (*A*), or *NLS-Smad1* (*N*). Whole cell lysates were immunoprecipitated with α-FLAG antibody followed by immunoblotting using α-Myc antibody to detect Smad4 in complex with Smad1. *F* and *G*, ventralization inducing activity of Smad1 in *Xenopus* embryos. *F*, *Xenopus* embryos at four-cell stage were injected with 500 pg of synthetic mRNA of wild-type, *Smad1*(*AVA*), or *Smad1*(*DVD*) into the dorsal marginal region. *G*, dorsal-anterior index of *Xenopus* embryos induced by Smad1. Values smaller than 5 indicate degree of ventralization.

adenovirus expressing Cre recombinase (pAxCANCre) or a human histone 2B-GFP unit (pAxH2BGFP) under control of the CAG promoter (22, 23). After being cultured for an additional 48 h, MEFs were transfected with plasmids using Lipofectamine 2000 (Invitrogen) in combinations as described in each figure legend. The cells were further cultured with or without BMP-4 before being examined for BMP activities as described below. A cell line, clone 16, was established by a limiting dilution method from *Smad4*$^{floxed/floxed}$ MEFs maintained by more than 30-fold serial passage. Bone marrow stromal cells were prepared from tibiae of 8-week-old *Smad4*$^{floxed/floxed}$ mice.

Immunohistochemistry, Immunoprecipitation, and Western Blot Analysis—The following antibodies were used for immunohistochemistry, Western blot analysis, and immunoprecipitation: anti-MHC antibody (clone MF-20, Developmental Studies Hybridoma Bank, Iowa City, IA), anti-myogenin (clone F5D, Santa Cruz, Santa Cruz, CA), anti-FLAG antibody (clone M2, Sigma), anti-Myc antibody (clone 9E10, Santa Cruz), anti-Myc polyclonal antibody (Medical & Biological Laboratories Co., Nagoya, Japan), anti-Smad4 antibody (clone B-8, SC-7966, Santa Cruz), anti-V5 antibody (P/N 46–0705, Invitrogen), anti-E4F1 antibody (Bethyl Laboratories, Montgomery, TX), anti-phospho-Smad1/5/8 polyclonal antibody (Cell Signaling, Beverly, MA), anti-Runx2/Cbfa-1 (Medical & Biological Laboratories Co.), and anti-β-actin antibody (I-19, SC-1616, Santa Cruz). For immunohistochemical analysis, target proteins were visualized using a Histofine SimpleStain Kit (Nichirei, Tokyo, Japan) or an Alexa 488- or Alexa 594-conjugated secondary antibody (Invitrogen). A BZ-9000 (Keyence, Tokyo, Japan) microscope was used for fluorescent analysis. Western blot analysis was performed as described (17). The target proteins were immunoprecipitated for 6 h at 4 °C using M2-agarose beads (Sigma). The target proteins were detected using a horseradish peroxidase-conjugated anti-mouse or anti-rabbit IgG antibody (GE Healthcare).

ALP and Luciferase Assays—ALP activity was stained as a typical marker of osteoblastic differentiation (24). Enzyme

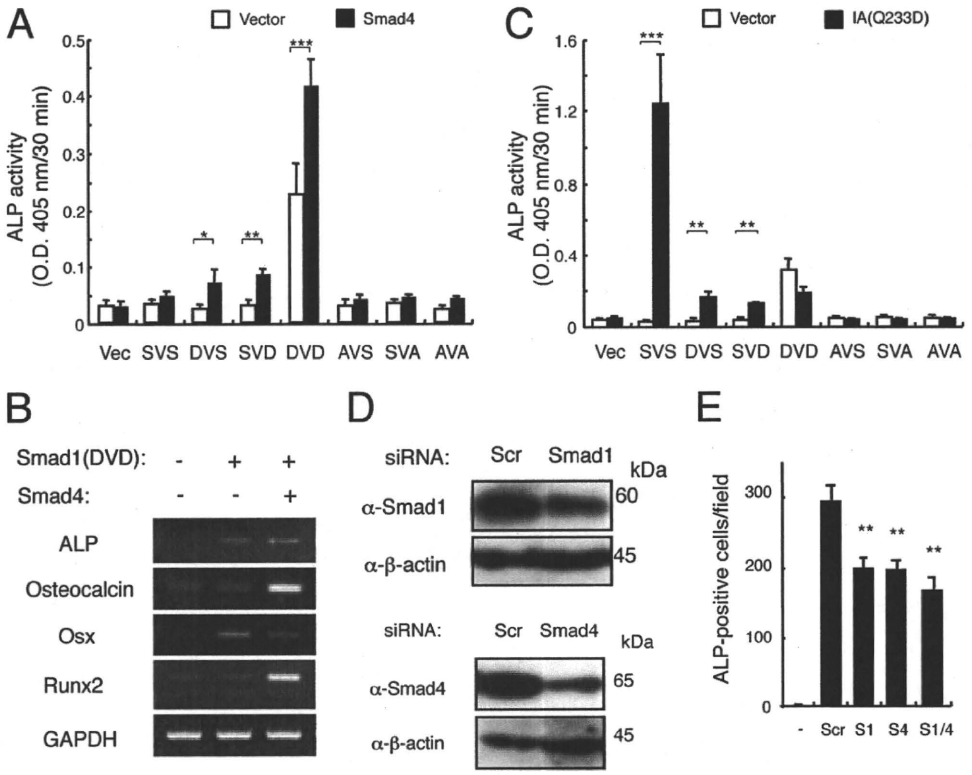

FIGURE 3. **Smad1(DVD) induces osteoblastic differentiation of C2C12 myoblasts.** *A*, Smad1(DVD) (*DVD*) induces ALP activity in C2C12 myoblasts. C2C12 cells were transfected with one of the *Smad1* constructs in the presence (*closed bars*) or absence (*open bars*) of *Smad4*, and ALP activity was measured on day 3. Values are mean ± S.D. ($n = 3$). *, $p < 0.05$; **, $p < 0.01$; ***, $p < 0.001$. *B*, Smad4 enhances Smad1(DVD) activity. C2C12 cells were transfected with empty vector alone or with *Smad1(DVD)* in the absence or presence of *Smad4*. Reverse transcription-PCR was performed on day 3. *C*, synergism between Smad1 and a constitutively activated BMPR-IA receptor. C2C12 cells were transfected with one of the *Smad1* constructs in the absence (*open bars*) or presence of *Bmpr-Ia(Q233D)* (*closed bars*), and ALP activity was determined on day 3. Values are mean ± S.D. ($n = 3$). *D*, knockdown of Smad1 and Smad4 in C2C12 cells. C2C12 cells were transfected with 20 nM *Smad1* (*upper panels*) and *Smad4* (*lower panels*) siRNA. Protein levels were determined by Western blots at 24 h. *E*, knockdown of Smad1 or Smad4 reduced ALP activity induced by BMP-4. The siRNA-transfected C2C12 cells were treated for 3 days with 100 ng/ml of BMP-4 and ALP activity was determined. Values are mean ± S.D. ($n = 3$). **, $p < 0.01$ compared with a scrambled siRNA transfection group.

activity was measured using *p*-nitrophenyl phosphate as a substrate (24). Luciferase assays were performed using pGL3MG-185 (25) or IdWT4F-luc reporter plasmids and phRL-SV40 (Promega, Madison, WI) with the Dual-Glo Luciferase Assay System (Promega) as described previously (13).

Dorsoventral Assay in Xenopus Embryos—A dorsoventral assay in *Xenopus* embryos was performed essentially as described (26). The injected embryos were allowed to develop until stages 34–40 for observation of external appearance and then subjected to histological analysis. The activity of each Smad1 was expressed by a dorso-anterior index (26, 27).

Reverse Transcription-PCR Analysis—Total RNAs were extracted using TRIzol (Invitrogen) and reverse transcribed with SuperScript III (Invitrogen). The PCR was performed using Platinum Pfx DNA polymerase (Invitrogen) as described (28). The primer sets used were previously described (29).

Chromatin Immunoprecipitation Assay—Cells were lysed in ChIP buffer (1% SDS, 10 mM EDTA, 50 mM Tris-HCl, pH 8.1) and sonicated. The chromatin solution was subjected to immunoprecipitation using a OneDay ChIP Kit (Diagenode, Sparta, NJ) according to the manufacturer's instructions. The following antibodies were used: anti-E4F1 (Bethyl), anti-Smad4 (sc-7966, Santa Cruz Biotechnology), anti-MyoD (sc-760, Santa Cruz Biotechnology), and anti-histone H3 (Upstate, Lake Placid, NY). The *Myogenin* promoter was amplified by PCR using the following primers: 5′-TAATTGAAAGGAGCAGATGAGACGGGG-3′ and 5′-CCATCAGGTCGGAAAAGGCTTGTTC-3′.

Statistical Analysis—Comparisons were made using an unpaired Student's *t* test. Results are represented as mean ± S.D. Statistical significance is displayed as: *, $p < 0.05$; **, $p < 0.01$; ***, $p < 0.001$.

RESULTS

Induction of the Smad-dependent Pathway by BMP-4 Regulates Both Myogenic and Osteoblastic Differentiation of C2C12 Cells—First, we determined the minimal culture periods of C2C12 cells with BMP-4 required for the inhibition of myogenic differentiation and induction of osteoblastic differentiation (Fig. 1*A*). Treatment of C2C12 cells with 100 ng/ml of BMP-4 for the first 30 min of a 3-day culture markedly suppressed myogenic differentiation on day 3 but did not induce ALP activity (Fig. 1, *B–E*). ALP-positive cells were detected in cultures treated with BMP-4 for longer than 9 h (Fig. 1, *B* and *E*). The BMP-4-induced inhibition of myogenic differentiation and induction of osteoblastic differentiation were blocked by Dorsomorphin, a BMP-Smad specific inhibitor, but not by inhibitors of mitogen-activated protein kinases, suggesting that the Smad-dependent pathway regulates conversion to differentiation (Fig. 1, *F–H*, and supplemental Fig. S1).

Construction of Constitutively Activated Smad1—We generated a series of Smad1 mutants, in which one or two serine residues at the carboxyl termini were substituted with aspartic acid or alanine residues (Fig. 2*A*). Among these Smad1 mutants, Smad1(DVD) exhibited transcriptional activity in a luciferase assay using the ID1 reporter without the addition of BMPs, and this activity was further enhanced by co-transfection with Smad4 (Fig. 2*B*). NLS-Smad1, in which a nuclear localization signal (NLS) was added to the amino terminus of Smad1, failed to induce luciferase activity. Smad1(DVD) was recognized by the α-phospho-Smad1/5/8 antibody, even in the absence of a constitutively active BMP receptor, BMPR-IA(Q233D), without affecting endogenous phospho-Smad1/5/8 levels (Fig. 2, *C* and *D*). Smad1(DVD) did not exhibit changes in cellular localization or interaction with Smad4 that were distinguishable from wild-type or other Smad1 mutants (Fig. 2, *D* and *E*). Injection of synthetic *Smad1(DVD)* mRNA into the dorsal sides

of *Xenopus* embryos induced ventralization, although *Smad1(AVA)* did not exhibit this activity (Fig. 2*F*). The average dorso-anterior index values induced by *Smad1(DVD)* and *Smad1(AVA)* were 1.79 and 5.00, respectively, indicating that Smad1(DVD) is a constitutively activated Smad1 in *Xenopus* embryos as well (Fig. 2*G*).

Activated Smad1 and Runx2, but Not Smad4, Cooperatively Induce Osteoblastic Differentiation of C2C12 Cells—Transient transfection of *Smad1(DVD)* in C2C12 cells induced expression of osteoblastic differentiation markers such as *ALP*, *Osteocalcin*, *Runx2*, and *Osterix*; this was further enhanced by the presence of *Smad4* for every marker except *Osterix*, which might be peaked within 3 days before sample preparation (Fig. 3, *A* and *B*). BMPR-IA(Q233D) stimulated ALP activity in cooperation with wild-type Smad1, confirming that Smad1 is a critical substrate of the type I receptor for induction of osteoblastic differentiation (Fig. 3*C*). However, no synergism was observed between BMPR-IA(Q233D) and any Smad1 mutants, including Smad1(DVD), suggesting that Smad1 mutants are not recognized as substrates by the receptor (Figs. 2*C* and 3*C*). Transfection of siRNA against *Smad1*, *Smad4*, or a combination of the two reduced the ALP activity induced by BMP-4 or BMPR-IA(Q233D) (Fig. 3, *D* and *E*). Similar results were obtained using siRNA against *Smad5* (data not shown).

The role of Smad proteins in osteoblastic differentiation was further examined using MEFs prepared from *Smad4*$^{floxed/floxed}$ mice. The MEFs had been infected with an adenovirus expressing Cre recombinase or EGFP *in vitro* before being treated with BMP-4. Western blot analysis revealed that the phosphorylation of Smad1/5/8 in response to BMP-4 was independent of Smad4 (Fig. 4*A*). In these MEF cultures, the ALP activity induced by BMP-4 was reduced but not eliminated in the Cre-expressing MEFs (Fig. 4*B*). We further examined the role of Smad4 in osteoblastic differentiation using bone marrow stromal/osteoblastic cells prepared from *Smad4*$^{floxed/floxed}$ mice. Again, *Smad4* was deleted *in vitro* by infection with an adenovirus expressing Cre, but expression of ALP was not eliminated in these cells; in fact, ALP expression was still induced by BMP-4 in a dose-dependent fashion in Smad4-deleted cultures (Fig. 4, *C* and *D*). These results suggested that Smad4 is not essential for BMP-induced osteoblastic differentiation but that it may enhance BMP signaling.

Runx2 is essential for osteoblast differentiation and also interacts with R-Smads (30–32). Overexpression of Smad1(DVD) or Runx2 alone induced ALP activity in C2C12 cells, and co-expression of Smad1(DVD) and Runx2 further increased ALP activity (Fig. 5*A*). In contrast, a dominant-negative form of Runx2 blocked ALP induction by Smad1(DVD) (Fig. 5*A*). RNAi knockdown of Runx2 reduced numbers of ALP-positive cells in C2C12 cultures induced by BMPR-IA(Q233D) (Fig. 5, *B* and *C*). Taken together, these findings suggest that phosphorylated R-Smads and Runx2 may cooperatively induce osteoblast differentiation in response to BMPs.

Smad4 Is Involved in Inhibition of Myogenic Differentiation by BMPs—We next examined the roles that the Smad signaling pathway plays in the inhibition of myogenic differentiation by BMPs. Overexpression of Smad1 mutants, including Smad1(DVD), did not inhibit the myogenic differentiation

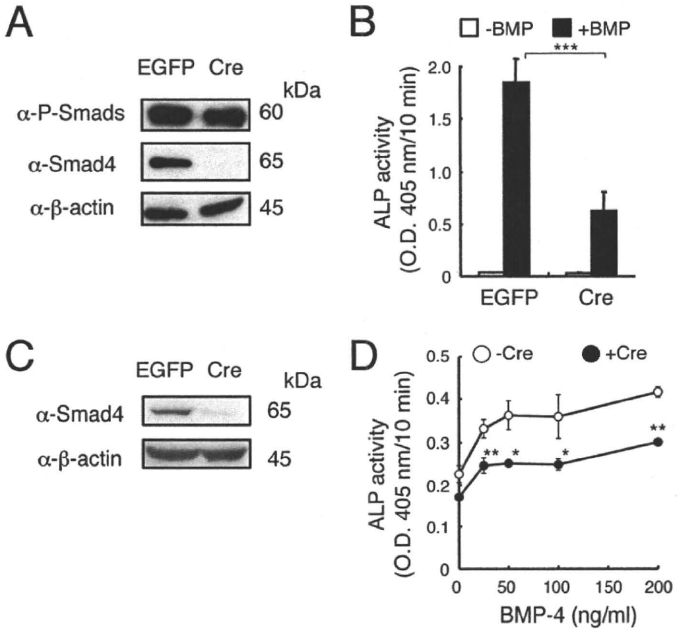

FIGURE 4. **Smad4 is not essential for the osteoblastic differentiation induced by BMP-4.** *A*, MEFs prepared from *Smad4*$^{floxed/floxed}$ were infected with adenovirus expressing Cre recombinase or EGFP. The cells were stimulated for 30 min with 100 ng/ml of BMP-4 to induce phosphorylation of Smad1/5/8. *B*, adenovirus-infected MEFs were treated for 3 days with 100 ng/ml of BMP-4, and ALP activity was determined on day 3. Values are mean ± S.D. ($n = 5$). ***, $p < 0.001$. *C*, Western blot analysis of Smad4-ablated bone marrow stromal/osteoblastic cells prepared from *Smad4*$^{floxed/floxed}$ mice. *D*, dose-dependent induction of ALP activity by BMP-4 in *Smad4*$^{floxed/floxed}$-derived bone marrow stromal/osteoblastic cells infected with Cre-expressing adenovirus or uninfected cells. Values are mean ± S.D. ($n = 3$). *, $p < 0.05$; **, $p < 0.01$.

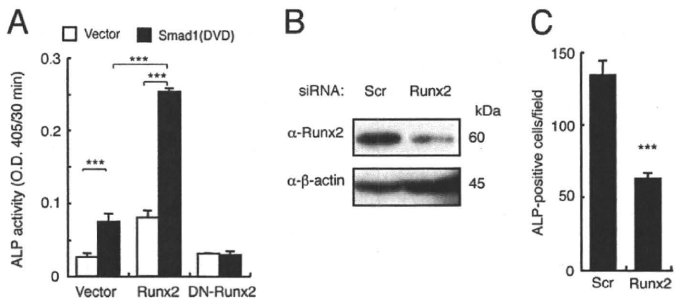

FIGURE 5. **Runx2 and Smad1(DVD) cooperatively induce osteoblastic differentiation of C2C12 cells.** *A*, C2C12 cells were co-transfected with *Smad1(DVD)* and *Runx2* or dominant-negative *Runx2*, and ALP activity was determined on day 3. Values are mean ± S.D. ($n = 3$). ***, $p < 0.001$. *B*, 20 nmol of *Runx2* siRNA or scrambled oligonucleotide was transfected in C2C12 cells, and protein levels were determined by Western blots at 24 h post-transfection. *C*, the siRNA-transfected C2C12 cells were co-transfected with *Bmpr-Ia(Q233D)* and *Smad1*, and ALP activity was determined on day 3. Values are mean ± S.D. ($n = 3$). ***, $p < 0.001$ compared with a scrambled siRNA transfection group.

induced by MyoD. Co-transfection of *Smad4* with *Smad1(DVD)* was required to reduce the number of MHC-positive cells (Fig. 6, *A* and *B*). This role of Smad4 in myogenic differentiation was confirmed in *Smad4*$^{floxed/floxed}$ MEFs. The transcriptional activity of MyoD was suppressed by BMP-4 in MEF cultures infected with a control virus (Fig. 6*C*). In contrast, the basal transcriptional activity of MyoD was increased ~1.4-fold in MEFs infected with the Cre-expressing adenovirus. This increase was not suppressed by BMP-4, suggesting that Smad4 is essential for the suppression of myogenic differentiation by BMPs

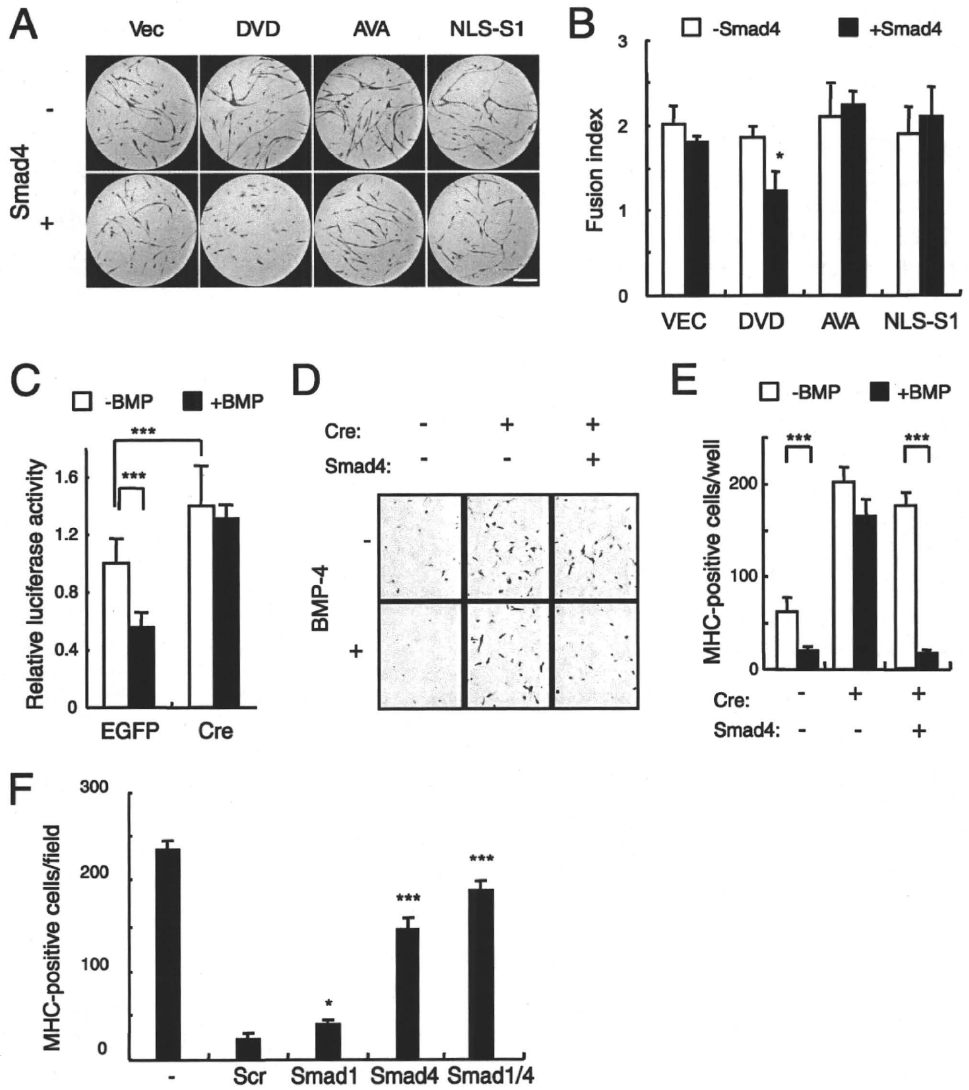

FIGURE 6. **Smad4 is involved in the inhibition of myogenic differentiation.** *A* and *B*, Smad1(DVD) inhibits myogenic differentiation only in the presence of Smad4. C3H10T1/2 fibroblasts were co-transfected with *MyoD* and empty vector (*Vec*), *Smad1(DVD)*, *Smad1(AVA)*, or *NLS-Smad1* (*NLS-S1*) in the absence (*upper panels*) or presence (*lower panels*) of *Smad4* (*A*). Myogenic cells were immunostained for MHC (*red*) on day 5. *Scale bar*, 400 μm. *B*, fusion index was determined in the presence (*closed bars*) or absence (*open bars*) of Smad4. Values are mean ± S.D. ($n = 3$). *, $p < 0.05$. *C*, Smad4 is required for suppression of transcriptional activity of MyoD by BMP-4. MEFs prepared from *Smad4*$^{floxed/floxed}$ were infected with adenovirus expressing EGFP or Cre recombinase, and then the transcriptional activity of MyoD was determined in the presence or absence of 100 ng/ml of BMP-4. Values are mean ± S.D. ($n = 10$). ***, $p < 0.001$. *D* and *E*, Smad4 is essential for inhibition of myogenic differentiation by BMPs. Clonal cell line 16 infected with Cre-expressing or EGFP-expressing control adenovirus was transfected with *MyoD* and stained for MHC on day 5 (*D*). *E*, the numbers of MHC-positive cells were counted in cultures prepared as in *D*. Values are mean ± S.D. ($n = 6$). ***, $p < 0.001$. *F*, 20 nmol of *Smad1* or *Smad4* siRNA or a scrambled oligonucleotide was transfected into C2C12 cells. These cells were treated with 100 ng/ml of BMP-4, and MHC-positive cells were counted on day 5. Values are mean ± S.D. ($n = 3$). *, $p < 0.05$; ***, $p < 0.001$ compared with a scrambled siRNA transfection group.

(Fig. 6*C*). This hypothesis was further confirmed using the floxed *Smad4* MEF cell line, clone 16. Transient transfection of MyoD in clone 16 induced a small number of MHC-positive cells, which were reduced in number by BMP-4 (Fig. 6, *D* and *E*). Infection by Cre-expressing adenovirus not only increased the number of MHC-positive cells, but also maintained this increase in the presence of BMP-4 (Fig. 6, *D* and *E*). Transient transfection of Smad4 in Cre-adenovirus-infected cultures restored the suppression of myogenic differentiation in response to BMP-4 (Fig. 6, *D* and *E*). Moreover, RNAi knockdown of Smad4 increased the number of MHC-positive cells in C2C12 cell cultures treated with BMP-4 (Fig. 6*F*). In contrast, knockdown of Smad1 had minimal effects on these cultures (Fig. 6*F*).

Inhibition of Myogenic Differentiation by Nuclear Smad4—Because Smad4 may translocate into the nucleus as a complex with Smad1/5/8 in response to BMP stimulation, we generated NLS-Smad4 and deletion mutants lacking amino-terminal MH1 (NLS-Smad4(ΔMH1)) and carboxyl-terminal MH2 (NLS-Smad4(ΔMH2)) domains, respectively (Fig. 7*A*). Nuclear localization of these NLS-Smad4 mutants was confirmed, although wild-type Smad4 was mainly detected in the cytoplasm (Fig. 7*B*). Overexpression of full-length NLS-Smad4 suppressed the myogenic differentiation of C3H10T1/2 cells induced by MyoD in a dose-dependent manner (Fig. 7, *C* and *D*, and data not shown). Unexpectedly, NLS-Smad4(ΔMH1), but not NLS-Smad4(ΔMH2), stimulated myogenic differentiation, suggesting that NLS-Smad4(ΔMH1) behaved in a dominant-negative fashion (Fig. 7, *C* and *D*). The Smad4 MH2 domain may thus interact with other molecules essential for inhibition of myogenic differentiation.

Involvement of E4F1 in the Inhibition of Myogenic Differentiation by BMP Signaling—We searched a protein-protein interaction data base that was constructed based on the mammalian two-hybrid method established by the RIKEN group (33) and found several proteins that formed complexes with Smad4. Among these proteins, we focused on E4F1, which contains six zinc fingers and a ubiquitin E3 ligase domain (Fig. 9*A*), because it appeared to be one of the transcription factors principally responsible for inhibition of myogenic differentiation by Smad4.

FLAG-tagged E4F1 was expressed in nuclei, co-localized with NLS-Smad4, and bound to larger amounts of NLS-Smad4 than wild-type Smad4 (Fig. 8, *A* and *B*). Interaction between endogenous Smad4 and FLAG-E4F1 was also detected in C2C12 cells (Fig. 8*C*). NLS-Smad4(ΔMH1), but not NLS-Smad4(ΔMH2), bound to E4F1, confirming that the complex is formed via the MH2 domain of Smad4 (Fig. 8*D*).

Both wild-type E4F1 and E4F1(ΔE3), but not zinc finger mutants, suppressed myogenic differentiation, suggesting that

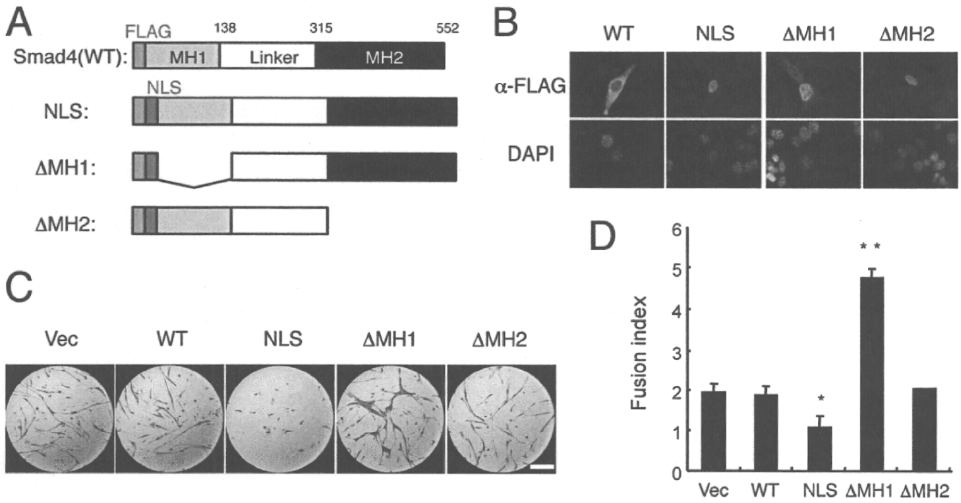

FIGURE 7. **Nuclear Smad4 inhibits myogenic differentiation.** *A*, scheme of construction of FLAG-tagged Smad4 mutants. *B*, cellular localization of FLAG-tagged Smad4 mutants. The cells were immunostained with α-FLAG antibody. *Scale bar*, 25 μm. *C*, effects of Smad4 mutants on myogenic differentiation. C3H10T1/2 cells were co-transfected with *MyoD* and one of the *Smad4* constructs and immunostained for MHC on day 5. *Scale bar*, 400 μm. *D*, fusion index was determined from cultures prepared as in *C*. Values are mean ± S.D. ($n = 3$). *, $p < 0.05$; **, $p < 0.01$. *DAPI*, 4′,6-diamidino-2-phenylindole.

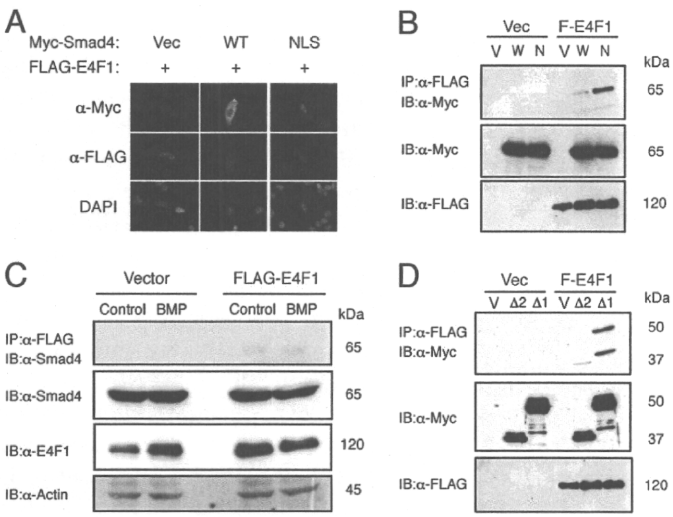

FIGURE 8. **E4F1 inhibits myogenic differentiation in cooperation with nuclear Smad4.** *A*, E4F1 and Smad4 overlapped in nuclei in C2C12 cells. FLAG-tagged *E4F1* and empty vector (*Vec*), *Myc-Smad4* (*WT*), or *Myc-NLS-Smad4* (*NLS*) were cotransfected and stained with α-Myc and α-FLAG antibodies. *B* and *C*, E4F1 interacts with Smad4 *in vivo*. *B*, COS-7 cells were co-transfected with *FLAG-E4F1* and empty vector (*Vec*), *Myc-Smad4* (*WT*), or *Myc-NLS-Smad4* (*NLS*). Whole cell lysates were immunoprecipitated (*IP*) with α-FLAG antibody followed by immunoblotting (*IB*) using α-Myc antibody. *C*, C2C12 cells transfected with *Flag-E4F1* were treated for 1 h without or with 100 ng/ml of BMP-4. Whole cell lysates were immunoprecipitated with M2-agarose beads followed by immunoblotting with antibodies for E4F1, Smad4, and actin. *D*, the MH2 domain of Smad4 is required for interaction with E4F1. The interaction between E4F1 and Smad4 was determined by cotransfection of *Flag-E4F1* and *Myc-NLS-Smad4*(*ΔMH2*) or *Myc-NLS-Smad4*(*ΔMH1*) in COS-7 cells. *DAPI*, 4′,6-diamidino-2-phenylindole.

E4F1 may inhibit myogenesis as a transcription factor rather than as a ubiquitin ligase (Fig. 9*B*). Although *Myogenin* is one of the targets of MyoD and is markedly suppressed by BMP signaling, we could not detect Smad4 or E4F1 binding to the *Myogenin* promoter in response to BMP-4 (supplemental Fig. S2). RNAi knockdown of E4F1 increased the number of MHC-positive C2C12 cells in the presence of BMP signaling (Fig. 9, *D* and *E*). Similar results were obtained using a plasmid-based microRNA expression vector for E4F1 (supplemental Fig. S3). We further examined the role of E4F1 in myogenesis in cell line clone 16 established from *Smad4*$^{floxed/floxed}$ MEFs. Again, deletion of *Smad4* by Cre-adenovirus infection increased the number of MyoD-induced MHC- and myogenin-positive myogenic cells (Fig. 9, *F* and *G*). Co-transfection of *Smad4* and *E4F1* markedly reduced the number of myogenic cells, suggesting that E4F1 acts cooperatively with Smad4 (Fig. 9*F*).

Id1–3 suppress myogenesis and are targets of BMP signaling. Transfection of *E4f1* increased Id1-, Id2-, and Id3-luc activities in C2C12 cells treated with and without BMP-4 (Fig. 9*G*, and data not shown). This stimulation by E4F1 seemed to be Smad4 dependent because the activity was lost by Smad4 ablation and restored by Smad4 overexpression in MEF clone 16 (Fig. 9*G*).

DISCUSSION

In the present study, we examined the molecular mechanisms underlying the conversion of myoblasts by BMPs, allowing their differentiation into osteoblastic cells. It has been suggested that a unique type of intracellular BMP signaling is involved in this conversion, because other inhibitors of myogenic differentiation, such as TGF-β and fibroblast growth factors, do not induce ectopic bone formation *in vivo* or osteoblastic differentiation *in vitro* (12). We found that the inhibition of myogenic differentiation by BMP-4 required treatment for less than 1 h, although induction of osteoblastic differentiation required treatment for more than 9 h. Both activities of BMPs were dependent on the Smad pathway, suggesting that related but distinct mechanisms regulate the conversion of myoblasts into osteoblastic cells. Because we failed to detect cells positive for both MHC and ALP in C2C12 cell cultures treated with BMPs (9, 12), it appeared that osteoblastic differentiation is activated only in immature myoblasts that have not yet initiated myogenic differentiation (34). This hypothesis was confirmed by our preliminary observation that BMPs did not induce ALP activity in mature multinucleated myotubes.[3]

BMP treatment can convert the differentiation pathway of myoblasts into osteoblastic cells and overexpression of constitutively activated BMP type I receptors such as BMPR-IA, BMPR-IB, and ALK2 can have the same effect without requiring the addition of BMPs (35, 36). However, we found that levels of endogenous Smad1 and Smad5 were low in C2C12 cells and that overexpression of wild-type Smad1 was required for induction of osteoblastic differentiation by BMPR-IA(Q233D). These findings suggested that downstream signaling of BMP type I receptors, rather than BMP type II and co-receptors,

[3] J. Nojima, T. Takada, and T. Katagiri, unpublished data.

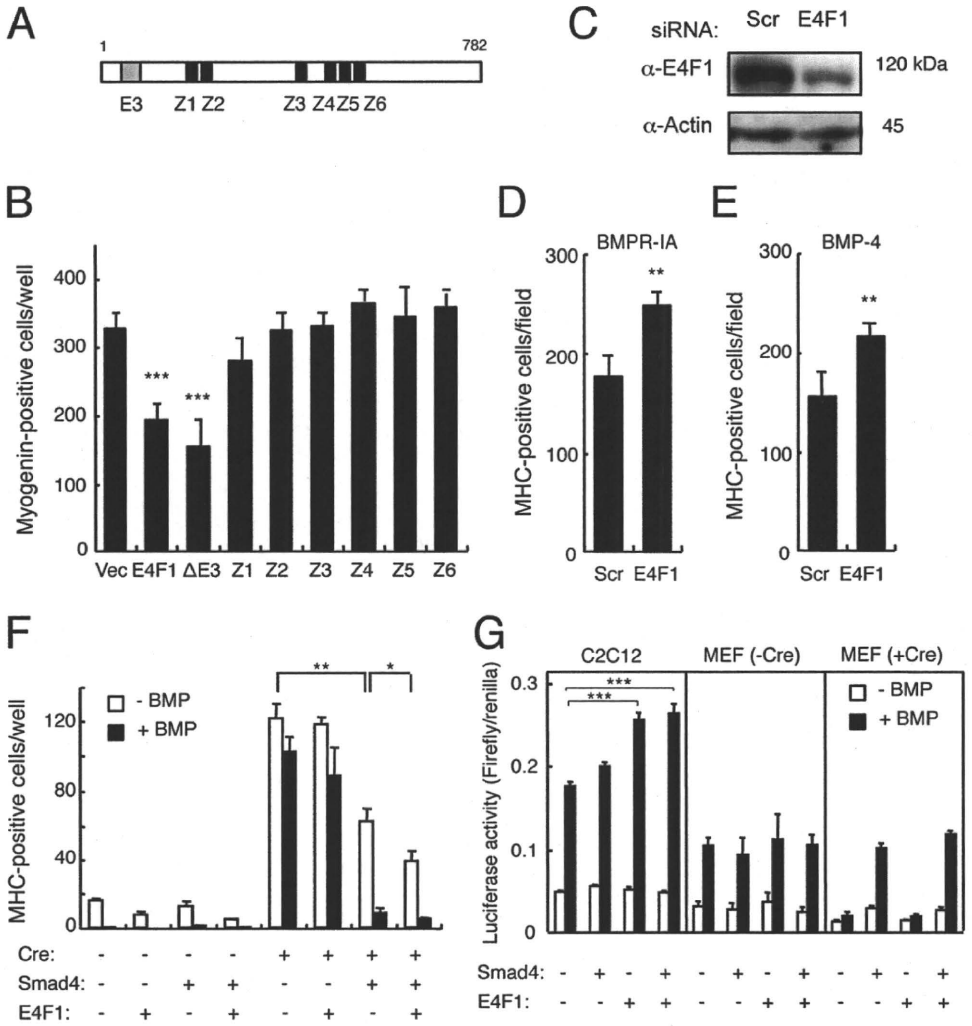

FIGURE 9. **E4F1 is involved in the BMP-induced inhibition of myogenesis.** *A*, schematic structure of E4F1. *E3*, an E3 ubiquitin ligase domain; *Z*, zinc fingers. *B*, overexpression of E4F1 inhibits myogenic differentiation. C3H10T1/2 cells were co-transfected with *MyoD* and wild-type *E4F1*, *E4F1*(*ΔE3*), or a zinc finger mutant *E4F1* and immunostained for myogenin on day 3. Values are mean ± S.D. ($n = 3$). ***, $p < 0.001$. *C*, 20 nmol of *E4F1* siRNA or scrambled oligonucleotide was transfected in C2C12 cells, and protein levels were determined by Western blots at 24 h post-transfection. *D* and *E*, the siRNA-transfected C2C12 cells were co-transfected with *Bmpr-Ia*(*Q233D*) (*D*) or treated with 100 ng/ml of BMP-4 (*E*), and MHC-positive cells were counted on day 5. Values are mean ± S.D. ($n = 3$). **, $p < 0.01$ compared with each scrambled siRNA transfection group. *F*, E4F1 suppresses myogenesis cooperatively with Smad4. *Smad4*$^{floxed/floxed}$-derived clonal cell line 16 was infected with or without a Cre-expressing adenovirus. The cells were transfected with or without *Smad4* in the presence or absence of Smad4, cultured with or without 100 ng/ml of BMP-4, and stained for MHC on day 3. Values are mean ± S.D. ($n = 3$). *, $p < 0.05$; **, $p < 0.01$. *G*, E4F1 stimulates *Id1* expression. C2C12 cells and MEF clone 16 infected with Cre adenovirus were transfected with *Id985-luc*, *E4F1*, and *Smad4* and were then cultured in the presence or absence of 50 ng/ml of BMP-4. Luciferase activity was determined on day 1. Values are mean ± S.D. ($n = 3$). *, $p < 0.05$; **, $p < 0.01$; ***, $p < 0.001$.

plays an important role in the conversion of myoblast differentiation. We established a constitutively activated Smad1, Smad1(DVD), to directly examine the role of the Smad pathway without activation of other signaling pathways induced by BMP receptors, such as the mitogen-activated protein kinase and phosphatidylinositol 3-kinase pathways. Serine residues were substituted with aspartic residues in Smad1(DVD) to introduce negative charges in the SVS motif at the carboxyl terminus, the site of phosphorylation by type I BMP receptors. These substitutions may induce conformational changes and stimulate interaction with coactivators such as p300, OAZ, and Runx2 (11). Indeed, Smad1(DVD) was directly recognized by the α-phospho-Smad1/5/8 antibody, suggesting that its three-dimensional structure is similar to that of native Smad1 phosphorylated by the receptors. We found that co-transfection of *Smad1(DVD)* with *Smad4* was capable of inducing osteoblastic differentiation of C2C12 myoblasts, and this induction was not inhibited by co-expression with Smad7, suggesting that Smad1(DVD) induces activation downstream of BMP type I receptors without activating endogenous BMPs or receptors. However, the ALP activity induced by Smad1(DVD) and Smad4 was lower than that induced by cotransfection of a constitutively activated BMPR-IA receptor and wild-type Smad1, although it was higher than that induced by BMPR-IA(Q233D) alone or Smad1(EVE), in which serine residues had been substituted with glutamic acids instead of aspartic acids.[3] These findings suggested that native phosphorylated Smad1 may have higher affinity for the coactivators required for osteoblastic differentiation than Smad1(DVD) or Smad1(EVE). This hypothesis will require further testing.

The Smad signaling pathway was also involved in the inhibition of myogenic differentiation. In contrast to osteoblast differentiation, however, this inhibitory activity of the Smad pathway appeared to be mainly dependent on Smad4 rather than R-Smads. In particular, the nuclear-targeted Smad4 markedly suppressed myogenic differentiation, although overexpression of NLS-Smad4 did not induce osteoblastic differentiation,[3] suggesting that Smad4 in complex with R-Smads inhibits myogenic differentiation after translocation from the cytoplasm to the nucleus in response to BMP stimulation. Because Smad4 is a common Smad among the TGF-β superfamily members, it may also be involved in mediating the effects of other myogenic inhibitors, such as TGF-βs, myostatin, and activin (37, 38).

The MH1 and MH2 domains of Smads have been shown to be involved in DNA binding and interaction with other proteins, respectively (39). Our deletion analysis suggested that nuclear Smad4 may interact with other transcriptional factor(s) and recruit them to the target DNA sequences via the MH2 and MH1 domains, respectively, to suppress myogenesis. This hypothesis was further supported by the finding of